T-4520

THE EFFECTS OF TEST CONDITIONS ON THE FRICTIONAL BEHAVIOR OF SHEET STEELS

by

John P. Haruff

A thesis submitted to the Faculty and Board of Trustees of the Colorado School of Mines in partial fulfillment of the requirements for the degree of Master of Science (Metallurgical and Materials Engineering).

Golden, Colorado
Date 30 MARCH 94

Signed: John P. Haruff

Approved: Thesis Advisor
Dr. David K. Matlock

Golden, Colorado
Date 3/30/94

Dr. John J. Moore
Professor and Head,
Department of Metallurgical and Materials Engineering

ABSTRACT

The frictional behavior of commercially produced electrogalvanized sheet steel with a nominal coating weight of 60 g/m^2 per side was evaluated with a laboratory bending under tension test system. Friction data were obtained with sliding speeds between 0.423 mm/s (1 in/min) and 42.3 mm/s (100 in/min) on rollers with diameters between 6.35 mm (0.25 in) and 50.8 mm (2.0 in) and were compared to similar results obtained on an uncoated section of the same commercial coil used to produce the coated product. The constant back force friction test method was used to generate multiple data pairs over the test range. Friction data were assumed to follow Amontons' (Columbic) friction theory in which calculated friction coefficients are pressure independent. The data of any given set of test parameters resulted in linear plots of adjusted pulling force versus back force with an intercept of zero. The linear plots indicate that Columbic friction appears to be applicable. For both the coated sheet steel and the bare steel substrate, measured coefficients of friction are essentially independent of die radius and contact pressure. The electrogalvanized sheet steel shows a significant increase in the coefficient of friction with a decrease in test speed. For the 50.8 mm diameter roller, the coefficient of friction increases from 0.24 to 0.55 when the speed decreases from 42.3 mm/s to 0.423 mm/s. This decrease in measured friction coefficient with increasing sliding speed is attributed to the strain rate sensitivity of the zinc coating since lubrication is most likely in the boundary regime for all test conditions. The decrease in zinc flow stress with a decrease in strain rate contributes to increased contact area, adhesion, and ploughing - all of which contribute to the friction force measured.

The repeatability and the uncertainty of the bending under tension friction test were evaluated. The repeatability of the test was confirmed by comparing data obtained on a cold rolled uncoated sheet steel tested previously to the results obtained on the current cold rolled

uncoated sheet steel. The two sets of data superimpose to identify a single value of the friction coefficient indicating that the frictional behavior is essentially constant for cold rolled sheet steel tested on the same die material using the same lubrication method. The uncertainty in the reported values of the friction coefficient was determined by applying the Kline-McClintock second power law to the friction equation. The results of this analysis indicated that the major contributor to the uncertainty in the friction coefficient is the measured forces. The typical values of measured forces result in reported friction coefficients plus or minus an uncertainty of 0.01.

TABLE OF CONTENTS

LIST OF FIGURES

LIST OF TABLES

ACKNOWLEDGEMENTS

I would like to thank the Advanced Steel Processing and Products Research Center for the financial and technical support of this research. Armco Steel Company was kind enough to donate the material examined in this project. I would also like to express my gratitude to Rocky Mountain Labs for the use of their profilometer.

My thesis committee members, Dr. D.K. Matlock, Dr. C.J. Van Tyne, Dr. G. Krauss, and Dr. R. Foley, deserve much praise for their insightful observations and stimulating discussions both of which brought this project to a level that could not be obtained without their input. I would also like to thank my colleagues for the meaningful interactions which broadened my knowledge far beyond what any class room instruction could.

And finally, I would like to express my gratitude to my family for their encouragement to pursue my academic desires because without their love and support none of this would have been possible.

1.0 INTRODUCTION

1.1 Friction and Formability of Coated Sheet Steels

In stamping of parts from zinc coated sheet steels, the formability depends on both the mechanical properties of the sheet and interactions at the sheet - tooling interface. The surface of the harder tool material contacts a sheet surface causing asperities of the softer zinc to deform. These surface interactions result in friction, adhesion and wear (1). The intent of the present study is to explain the frictional behavior of electrogalvanized sheet steel as a function of tooling geometry and processing speed. The frictional behavior of zinc coated sheet steels is complex and is influenced by many variables such as: coating, substrate and tooling properties; surface characteristics of the workpiece and tool; lubrication; and imposed interfacial conditions. These variables and their effect on the frictional behavior on sheet materials are examined below in Section 1.3 of this thesis. The present work extends previous work of sheet metal formability (2-4) at the Colorado School of Mines.

Electrogalvanized sheet steel was chosen for this study because of its extensive usage in the automotive industry. The corrosion resistant properties of an electrogalvanized steel makes it the material of choice in many applications. Unfortunately, galvanized sheet steels generally exhibit inferior press shop performance when compared to uncoated sheet steel (5). The present study relates the forming variables of die radius and displacement rate to the frictional behavior of electrogalvanized sheet steel in order to address some issues which may lead to poor press shop performance of electrogalvanized sheet steels. An uncoated aluminum-killed drawing quality cold rolled sheet steel, which serves as a reference material, is also examined in the present study.

1.1.1 Friction

Friction is defined as "a force which is tangential to the common boundary of two bodies in contact and which resists the motion or tendency to motion of one relative to the other" (6). The frictional resistance results from surface asperity deformation (a function of contact pressure, lubrication, surface morphology, surface mechanical properties, *etc.*) and molecular interactions between two bodies (1).

Friction in forming operations is a means of transferring forces from the tooling to the workpiece to impose plastic deformation of the workpiece. Friction can have a profound influence on the forming operation and is often instrumental in the successful or unsuccessful production of a part. Control of friction during a forming process often results in a final part which exhibits the desired shape, appearance and mechanical properties (7). Uncontrolled friction can cause localized stress concentrations which may result in fracture, poor surface characteristics and degradation of the localized mechanical properties in the sheet (7).

The significance of surface asperity deformation on friction forces which develop at the interface between two sliding surfaces is illustrated in the schematic drawing in Figure 1.1 which is adapted from Schey (1) and shows the mechanical interaction of the tool and workpiece asperities. The interaction between the two surfaces must be overcome in order for sliding to continue. Schey (1) also notes that chemical bonding between surfaces in intimate contact can contribute to interfacial friction. If close interaction of two solid bodies results in interatomic forces and/or cold welding at the tool - workpiece interface, the bonds must be broken before sliding can continue. The making and breaking of interface welds can

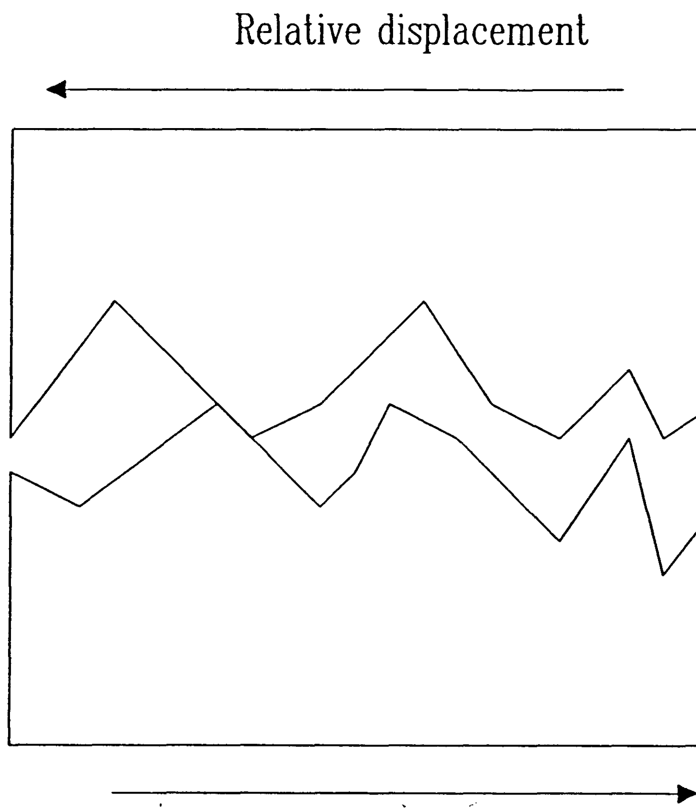

Figure 1.1 Schematic representation of asperity interaction of sliding bodies. (1)

lead to galling which results in material adhering to the die and an increase in the tool - workpiece interactions.

There are two common methods of describing the stress due to friction, τ: Amontons' friction (a.k.a. Columbic friction) and constant friction factor. Amontons' theory will be described followed by a discussion of constant friction factor theory. Both friction theories have been applied to sheet metal forming operations and the conditions to which each theory applies are addressed below.

The two basic features of friction as defined by Amonton are: 1) the frictional force is proportional to the normal force, and 2) the frictional force is independent of the size of the apparent contact area. When both of these conditions are satisfied the measured friction is often referred to as Columbic friction (1,8). The coefficient of friction, μ, from a mechanical engineering definition is often written as (1):

$$\mu = \frac{F}{P} = \frac{\tau}{\sigma} \qquad [1.1]$$

where: F = the force required to move a body over the surface

P = the normal force between the two bodies

τ = the sliding shear stress

σ = the stress perpendicular to the sliding surfaces

The coefficient of friction, μ, has a maximum value of 0.577 for a material which obeys the von Mises yield criteria (1,8). This maximum occurs when the normal stress, σ, eventually reaches significantly high levels that it is preferable for the material to shear internally rather than slide along the external surface.

The basis for the constant friction factor theory is that the frictional shear stress, τ is some fraction of the shear strength of the material. Implicit with in this approach to friction is the fact that τ is independent of the normal stress, σ. A mathematical description of the constant friction factor, m, is be defined as:

$$m = \frac{\tau}{k} \qquad [1.2]$$

where: τ = the frictional stress at the interface of the two materials sliding relative to each other

k = the shear flow stress of the material which under goes plastic deformation

The allowable values for m range from 0.0 for a frictionless interface to 1.0 for complete sticking when von Mises yield criteria is assumed. Under the assumption of von Mises yield criteria, k is $\sigma_o/\sqrt{3}$ where σ_o is the flow stress for the material in simple tension.

The two friction descriptions, Columbic and constant, are presented in Figure 1.2 as a plot of interfacial shear stress versus normal contact pressure (1). Columbic friction is indicated by the dashed lines which have a slope of μ and an intercept of zero. The constant friction regime has a slope of zero and a y-axis intercept of $\sigma_o/\sqrt{3}$ when m=1.0. The

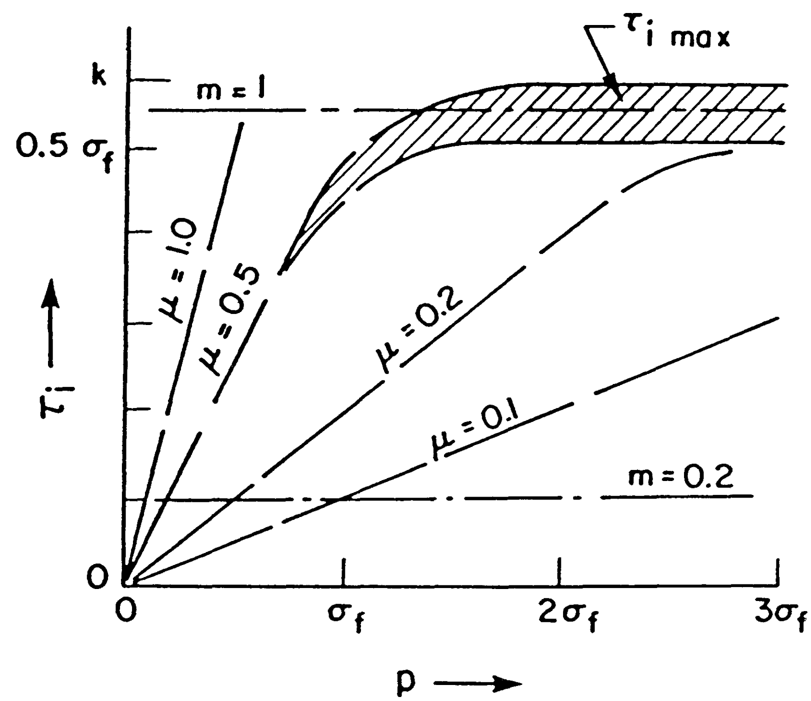

Figure 1.2 Graphical representation of two friction theories - Columbic friction and constant friction factor. Columbic friction is indicated by the dashed lines and constant friction by the solid lines (1).

Columbic theory has been shown to be a better model for interfacial friction at lower normal contact pressures while constant friction factor better models frictional behavior at higher contact pressures (8).

1.2 Methods of Friction Testing for Sheet Materials

In order to determine the frictional behavior of sheet materials, several test methods have been proposed and have met with varying success. A few of the more common tests are: the flat die sliding test (9), the draw bead simulator (DBS) (10), the tensile strip test (11) and the bending under tension test (BUTT) (12). Schematic drawings for each of these tests are shown in Figures 1.3 to 1.6 respectively. Each of these friction tests have three common elements: two materials in contact; an applied force which displaces one material with respect to the other; and the presence of a normal force which creates a frictional condition at the interface (13). To determine the friction coefficient, both the force required to cause sliding and the normal force must be measured. Each friction test has benefits as well as disadvantages when compared to other test methods.

Friction is a system parameter, *i.e.* a property that depends on the test method used and not a true material property which would be independent of test method (1). Measured friction coefficients depend on the material of the workpiece and tooling as well as the processing conditions (*i.e.* lubrication, tool geometry, speed, *etc.*). Hence, measured values of friction depend directly on the test method employed. Furthermore, Ranta-Eskola *et al.* (14) have shown that frictional values determined by different test methods should not be directly compared.

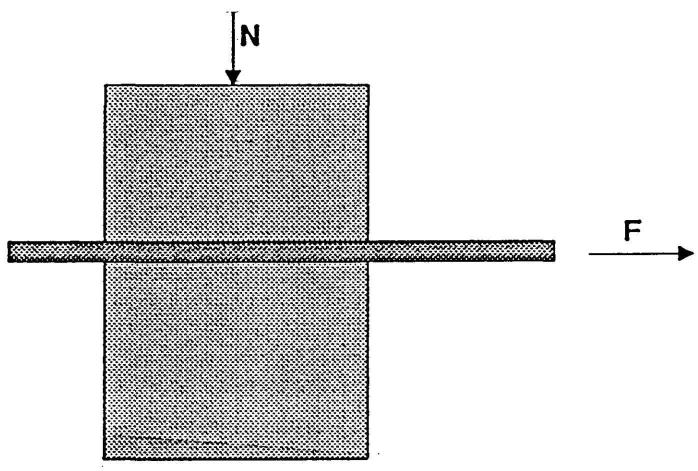

Figure 1.3 A schematic representation of the flat die sliding friction test. The forces measured to determine friction are F, the pulling force and N, the normal force.

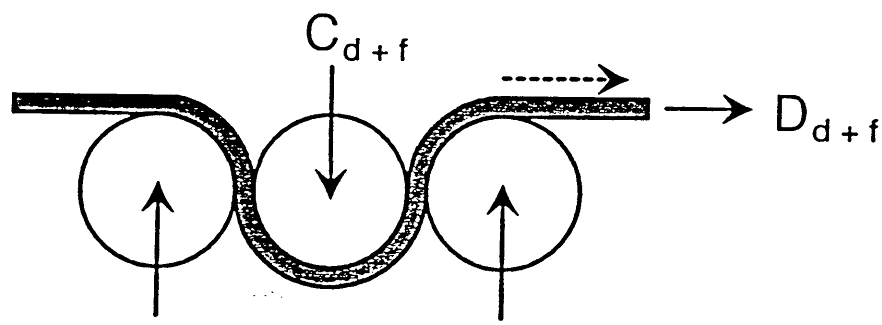

Figure 1.4 A schematic drawing of a draw bead friction test. The measured forces are D_{d+f}, the drawing force and C_{d+f}, the clamping force.

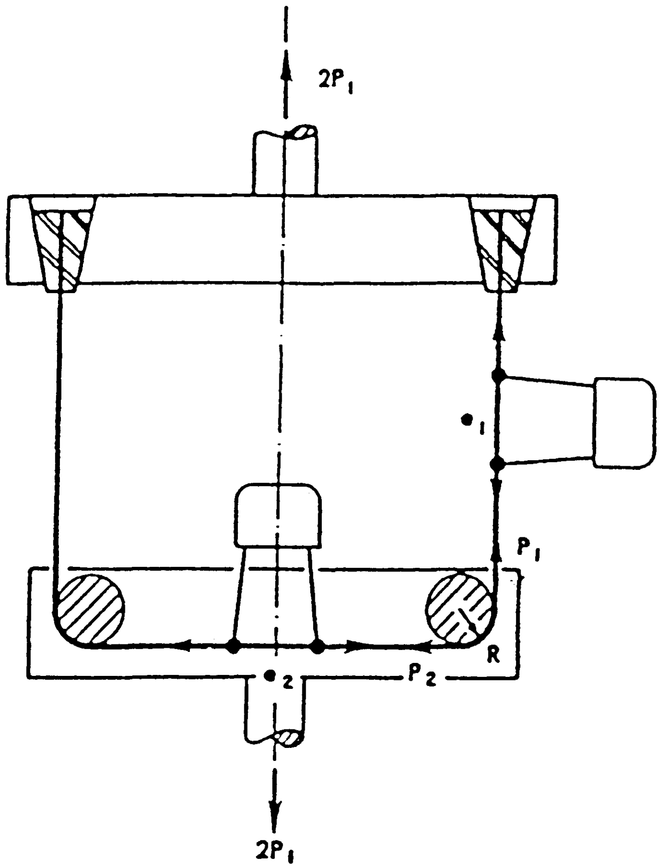

Figure 1.5 A schematic drawing of the tensile strip friction test. The measured force is $2P_1$. (15)

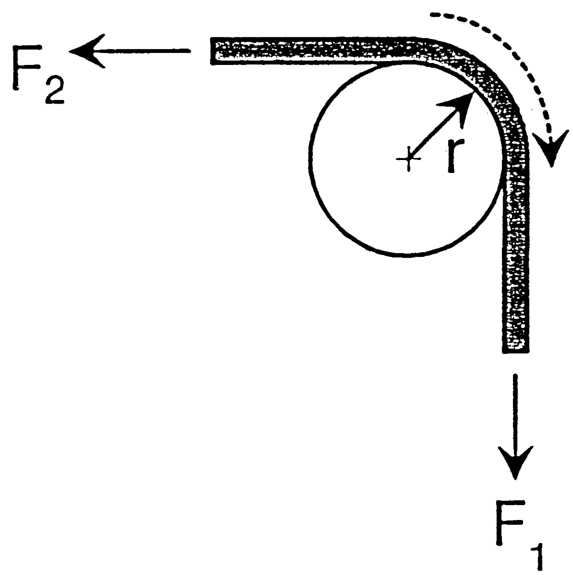

Figure 1.6 A schematic drawing of the bending under tension friction test. The measured forces are F_1 the pulling force and F_2 the back force.

The friction test used to evaluate a sheet material is dictated by the forming conditions that are of interest. For example the frictional behavior in draw beads may be of interest and the use of a particular test may be appropriate while the same friction test may not be a good test to model friction over a punch nose. The most basic friction test is the Wojtowicz flat die sliding test shown schematically in Figure 1.3. In this test both the tool and workpiece experience elastic deformation. The measured forces are F, the pulling force, and N, the normal force. Based on the dimensions of the blocks and the measured forces, an average coefficient of friction can be determined for both sides of the sheet. If the coefficient of friction of only one side of the material is of interest, one of the backing blocks is allowed to move with the sheet. For the conditions shown in Figure 1.3, the coefficient, μ, is determined by the following equation:

$$\mu = \frac{F}{2N} \tag{1.3}$$

where: F = the pulling force

N = the normal force

Since both sides of the sheet contribute to the measured force value, the 2 appears in the denominator. This test, in which the sheet experiences only elastic deformation, is not realistic for forming operations where plastic deformation of the sheet occurs (14).

A common method to determine the friction coefficient relevant to sheet forming processes is the draw bead simulator or DBS test (10). In this test the sheet material is subjected to loading conditions and strain paths that simulate those found in draw beads which are used to control the flow of material into dies during stamping operations (12). A schematic drawing of a draw bead test is shown in Figure 1.4. The DBS test has provisions to eliminate bulk material properties which allows surface interactions to be isolated. This is done by drawing a strip through the fixture while the beads are allowed to rotate freely. The resultant drawing force measurement is the force required to bend and unbend the strip. The material under investigation is then drawn through the apparatus while the beads are locked in place and the forces required to overcome friction in addition to the force required to bend and unbend the strip are measured. If the pressure between the draw bead and sheet is assumed to be constant, the coefficient of friction is obtained (10) from:

$$\mu = \frac{D_{d+f} - D_d}{\pi C_{d+f}} \qquad [1.4]$$

where: D_{d+f} = the measured drawing force for the fixed beads

D_d = the measured drawing force for the free rolling beads

C_{d+f} = the measured clamping force

The DBS test takes into account friction on both sides of the sheet. However, by replacing the center draw bead in Figure 1.4 with a freely turning roller, it is possible to determine the friction on one side of the sheet through the desired DBS.

Marciniak developed a friction test to simulate friction conditions at a punch nose, which is called the tensile strip test (11). The tensile strip test is shown schematically in

Figure 1.5. The pulling force and the sliding force are a result of the loading force $2P_1$ as shown in Figure 1.5. The tooling consists of two cylindrical dies of the desired radius, R, which are rigidly held and do not rotate and the relative sliding between the tool and workpiece results from displacement of the cross-head. Strains are measured with extensometers in each of the sheet metal ligaments (15) and with knowledge of the engineering stress - strain behavior of the material, the loads in each ligament are determined. From the measured data the coefficient of friction can be calculated from:

$$\mu = \frac{2}{\pi} \ln \frac{P_1}{P_2} \qquad [1.5]$$

where: P_1 and P_2 are loads in the ligaments of the sheet

The tensile strip test has the advantage of being able to measure friction on one side of the sheet. This is especially important if frictional differences between the two sides of coated sheet steels exist. As is the case in the DBS test, the material experiences significant plastic flow during testing. However, in the tensile strip test the average friction coefficient for the two cylindrical tool surfaces is determined. In the tensile strip test, the relative speed between the tool and workpiece approaches zero and the force due to bending is ignored. The process of averaging the frictional behavior over two dies may introduce errors since each die - sheet interface may not be identical due to slight differences in the tool surfaces or uneven lubrication. The relative speed between the tool and the workpiece experienced in the tensile strip test is not representative of actual speeds encountered in stamping operations. Also, the strip is bent to its final shape before testing and by ignoring the bending force errors in calculated friction coefficients may be introduced.

The final friction test method to be described in this section is the bending under tension friction test (12) shown schematically in Figure 1.6. The bending under tension friction test has several advantages when compared to the previous tests (12,16-18) and as a result is used for the friction measurements in this thesis. The test itself, as well as the advantages and disadvantages are described below.

The bending under tension friction test consists of drawing a sheet specimen over a cylindrical die and measuring the resultant forces. The test is preformed in two stages. First the bending force is determined for a specific roller diameter with either a free roller test (12) or an extrapolation method (19). Second, the force required to overcome friction is determined with a fixed roller test (12). The bending under tension test is normally performed with a constant back force. The constant back force method incorporates data pairs from multiple tests at different back forces for both free and fixed roller tests.

In the free roller test, two assumptions are made: first there is no sliding between the sheet sample and the roller at the interface, and secondly the friction due to the bearings is negligible in determining the bending force. With these assumptions the difference in measured front and back forces is the bending force required to bend the sheet so that it conforms to the roller. The extrapolation method of Davies and Stewart (19) determines the bending force by the y-axes intercept from a plot of pulling force verses back force for a fixed roller test. In the Davies and Stewart method the fixed roller force data are extrapolated back to a pulling force of zero and the intercept is the theoretical bending force for the material over a specific die radius. This technique is illustrated in Figure 1.7.

In the fixed roller test, the sample slides over the roller and the difference in the measured front and back forces is the force required to overcome sliding friction as well as the force required to bend the sheet so that it conforms to the roller.

For the bending under tension friction test

$$\mu = \frac{1}{\theta}\left(\frac{r+0.5t}{r}\right)\ln\left(\frac{(F_1-F_b)/F_y}{F_2/F_y}\right) \qquad [1.6]$$

where: θ = angle of wrap
r = roller radius
t = sheet thickness
F_1 = pulling force
F_2 = back tension force
F_b = bending force
F_y = strip yield force

The friction coefficient, μ, can be calculated using Equation 1.6, which is comprised of a geometric factor and a force factor (12,13). The mathematical relationship in Equation 1.6 can be derived either from a energy balance or a force balance approach (2). The variables r (roll radius) and t (sheet thickness) depend on test geometry and the specific material respectively and along with the angle of wrap (for the tests conducted as part of this thesis, $\theta = 90°$ or $\pi/2$) comprise the geometric term of Equation 1.6. The force data pairs, from multiple back forces at each set of test parameters, are then plotted as shown in

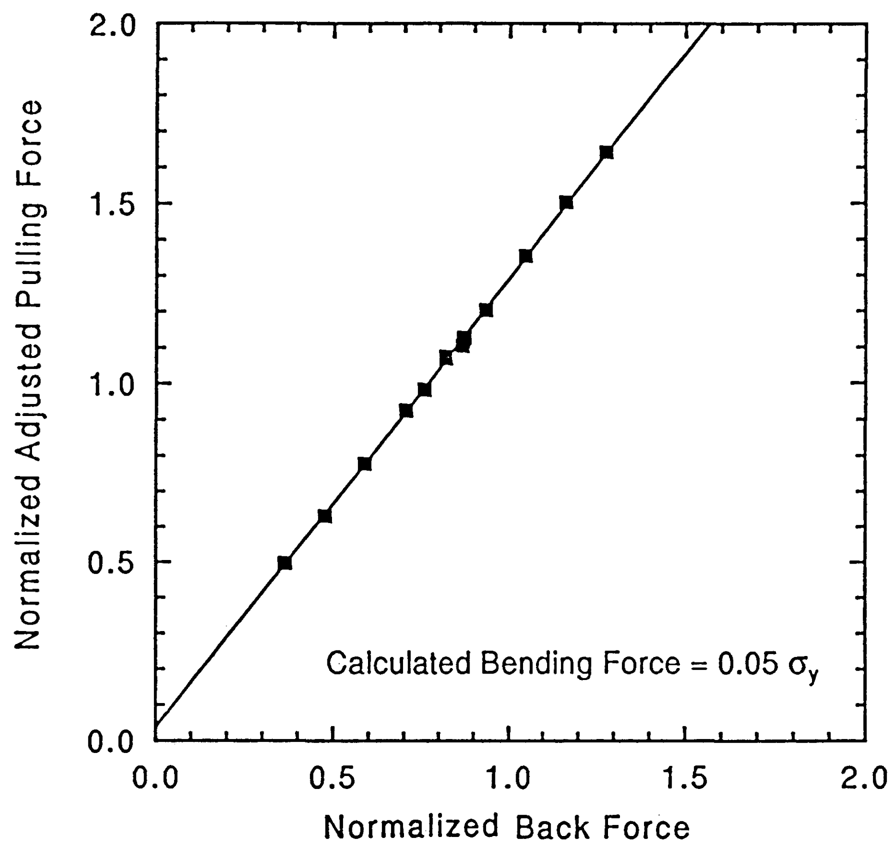

Figure 1.7 An example of the Davies and Stewart (19) method to determine the bending force. The extrapolation method determines that the bending force at the y-axis intercept in a pulling versus back force plot.

Figure 1.8. The forces are normalized by the force required to yield the strip in pure tension, F_y. The argument of the logarithm (*i.e.* the force term, in Equation 1.6) is the slope of the normalized adjusted pulling force, $(F_1 - F_b)/F_y$ versus the normalized back force, F_2/F_y. This slope is then used to determine the friction coefficient for given test conditions. The analysis assumes Columbic friction theory. This assumption implies that the coefficient of friction, μ, is not a function of pressure and that μ is constant along the line of contact.

1.3 Factors that Affect Friction in Sheet Metal Forming

The frictional behavior of zinc coated sheet steels is complex and influenced by a number of variables: the physical and mechanical properties of the coating, substrate and die materials; the surface morphology of both the coating and the die materials; the lubricant; and the imposed interfacial loading conditions which include contact pressure, interfacial temperature and relative sliding speed (16). In the present study the factors investigated are forming speed and tool geometry, especially their effect on measured friction coefficients. Lubrication response depends in part on these two factors (1) and will be briefly addressed in this section.

1.3.1 Material Properties and Their Effect on Friction

Both substrate and coating properties influence the friction coefficient. Substrate properties such as yield strength and ductility determine the strains, both elastic and plastic, that occur within the coating during forming. The substrate surface morphology also is

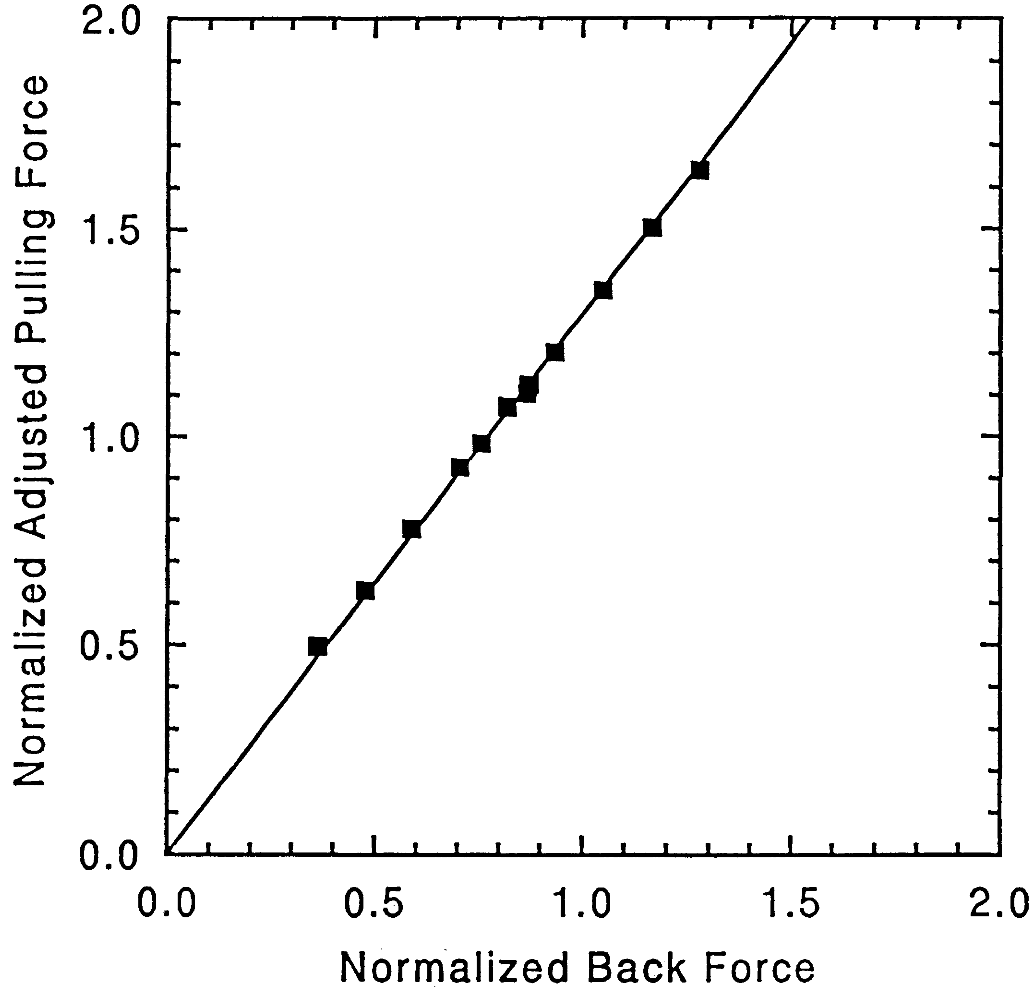

Figure 1.8 Force data pairs from multiple fixed roller bending under tension friction tests are plotted as normalized adjusted pulling force versus normalized back force.

important since it influences the final coating crystallographic texture, roughness, *etc.* which will affect the friction during forming operations (20).

The coating properties are also important because the interaction between the coating surface and the tooling surface ultimately determines the frictional behavior. The effects of variations in zinc coating properties, such as grain size, impurity alloy content, crystallographic texture, and roughness have been considered in several recent publications (21-25) and are considered more completely by Wenzloff *et al.* (26). To date, the development of a definitive relationship between a single specific coating property and friction has been elusive. For example, Hashimoto *et al.* (24) found that the coefficient of friction (μ) decreased as the average arithmetic roughness (R_a) increased for electrogalvanized material, while Wenzloff *et al.* (26) found that μ increased with increasing roughness. Kumpulainen (25), in contrast, reported no significant dependence of the coefficient of friction on surface roughness.

The flow behavior of the coating is controlled by coating strength and crystallographic texture. Crystallographic texture, which for a pure zinc coating is characterized as pyramidal, prismatic, or basal, has been shown to correlate directly to the frictional behavior of materials (24). For example, Rangaragan (21) and Wenzloff (3) showed that materials with prismatic textures tend to exhibit lower friction coefficients. This observation is in direct contrast with the results of Buckley and Johnson (27) who indicated that basal textured coatings exhibit lower friction coefficients. With respect to coating hardness, Iway *et al.* (28) found that measured friction coefficients decreased with an increase in coating hardness.

Changes in crystallographic texture and coating hardness control the deformation behavior of the coating and correspondingly the degree of asperity deformation at a specific contact pressure. In the presence of a lubricant, friction depends on the true contact area (29,30), defined as the sum of the areas associated with flattened asperities. Recent literature shows a contradiction in findings for the relationship between friction and true contact area. Wilson (29) found that for electrogalvanized steels, the friction coefficient increases with an increase in the true contact area. Meier and Reissner (30) showed that the coefficient of friction decreased with an increase in surface contact pressure which should be directly related to contact area. If the true contact area were the only parameter which controlled friction, then measured friction coefficients should depend on contact pressure as contact area increases with contact pressure. However, recent data obtained with the bending under tension friction test (2,12,22,23,26) have shown that in many cases, measured friction coefficients do not appear to depend on contact pressure.

In addition to the coating properties, the type of lubricant as well as the lubrication regime also affect the frictional behavior of zinc coated sheet steels during forming. The key elements that determine the lubrication regime in a forming operation include the amount of lubricant, lubricant chemistry, lubricant viscosity, surface roughness of both the sheet and the tooling, contact pressure and the relative velocity between the workpiece and the tool. The lubrication regime can be divided into four regions as described by Wilson (31). The categories, listed in order of increasing lubrication are: boundary, mixed, thin film, and thick film. A typical Stribeck curve, Figure 1.9, illustrates these regions (32), where the hydrodynamic region consists of the thin and thick film categories noted by Wilson.

Increasing lubrication results in a decrease in asperity contact and correspondingly a decrease in contact area at a given contact pressure. In most stamping operations the lubrication will be in the boundary region. The movement into the hydrodynamic region would only occur at extremely high speeds which are not obtained over the entire stroke length of a mechanical stamping press.

In laboratory evaluations of friction, one parameter, the relative speed between the sheet and the die, is usually held constant. However, as described by the H factor ($\eta v/p$) in the Stribeck curve (1) the relative velocity and pressure determines the specific lubrication regime which develops at the workpiece-tool interface assuming a constant lubricant viscosity. Measured friction coefficients in laboratory friction tests have been shown to decrease with an increase in test speed (25,33-37). The decrease in measured coefficients of friction is illustrated in Figure 1.10 by the research done by Nakamura *et al.* (35). In contrast Wilson found that the measured friction coefficient was not a function of sliding speed in a study of AKDQ sheet steel as shown in Figure 1.11 (29) and there is no reference found in the literature that the coefficient of friction increases with sliding speed.

Another friction test parameter usually held constant is the tool geometry. The combination of applied loading and tool geometry determine the contact pressure at the tool - workpiece interface. However, the mechanical properties of the sheet usually are the limiting factors in contact pressure. To increase the contact pressure at the interface, the simplest method is to reduce the tool radius for cylindrical tooling. The contact pressure can be

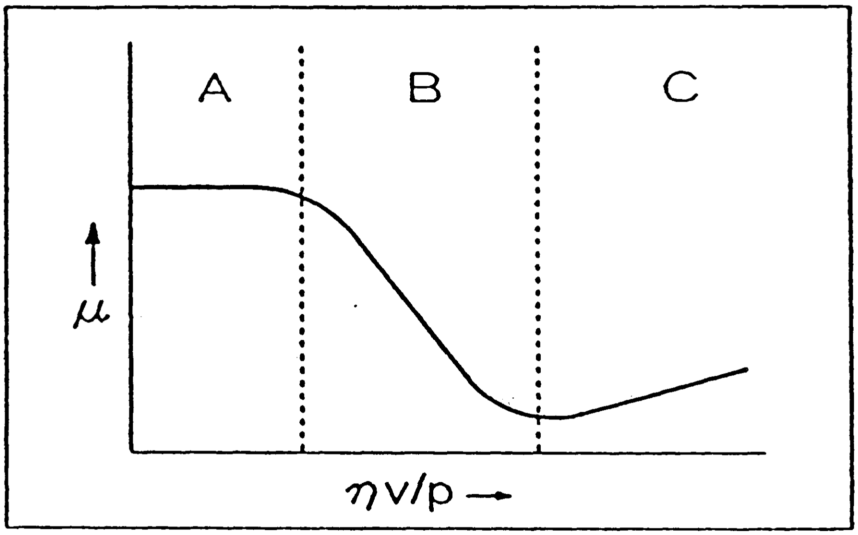

Figure 1.9 A schematic drawing of a typical Stribeck curve. The curve is divided into three regions: A) boundary lubrication, B) mixed lubrication and C) hydrodynamic.

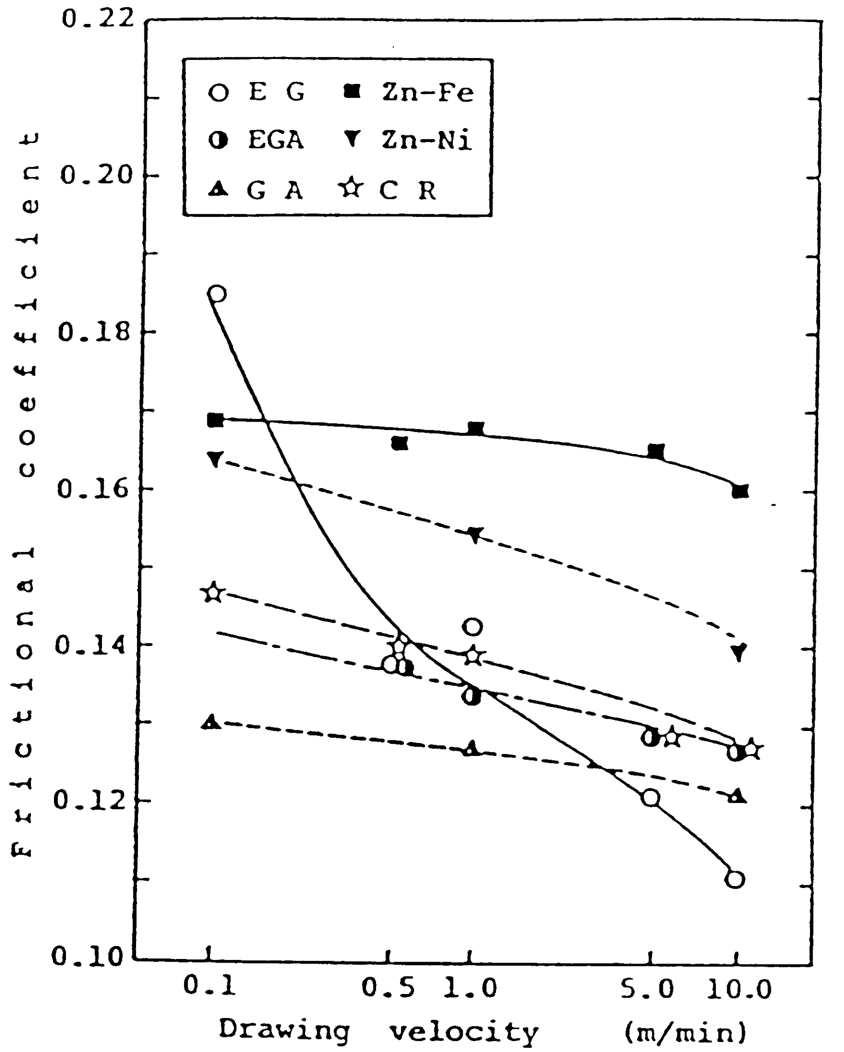

Figure 1.10 A plot of coefficient of friction versus drawing velocity for several different coated sheet steels as well as an uncoated sheet steel tested by Nakamura *et al.* (34).

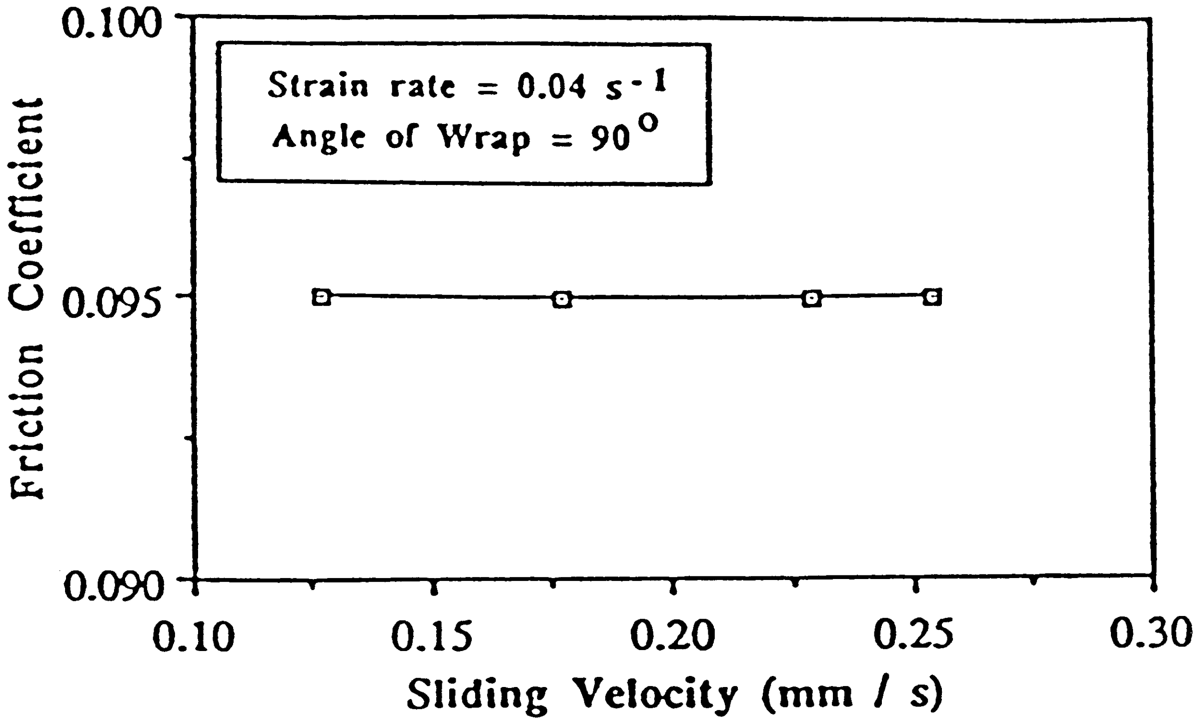

Figure 1.11 Wilson found that the coefficient of friction was not influenced by the relative speed between the tool and an AKDQ sheet steel test sample (29)

calculated and the precise equation is test dependent. In all cases it is found that the pressure is inversely proportional to the tool radius, *i.e.*

$$p \propto \frac{1}{R} \qquad [1.7]$$

where: p = the average contact pressure

R = the radius of the cylindrical tool

Recent literature shows that the correlation between contact pressure (or die radius) and measured friction is not clear. Several researchers (25,29,34,35,38) have shown that the measured friction stress increases with increasing contact pressure as shown in Figure 1.12, for an AKDQ material studied by Wilson (29). Note the similarities to Figure 1.2, the friction stress as a function of pressure for the Columbic and constant friction factor theories. The opposite trend has also be observed in other friction testing studies (30,39,40). The current thesis addresses this issue of the relationship between contact pressure and friction coefficient by changing the die radius in the bending under tension friction test apparatus.

To date limited results have been presented to correlate test conditions, such as test speed and contact pressure, with the fundamental deformation behavior of the coatings. In order to obtain a complete understanding of friction in forming operations, an understanding of the interrelationships between the coating properties and test conditions must be determined. In the present work a systematic analysis of the effects of test speed and contact pressure on the frictional behavior of a commercially produced electrogalvanized sheet steel is developed. Data on the zinc coated sheet steel are obtained with the bending under tension friction test and are compared with similar data obtained on the uncoated steel substrate from the same coil used for the coated sheet steel.

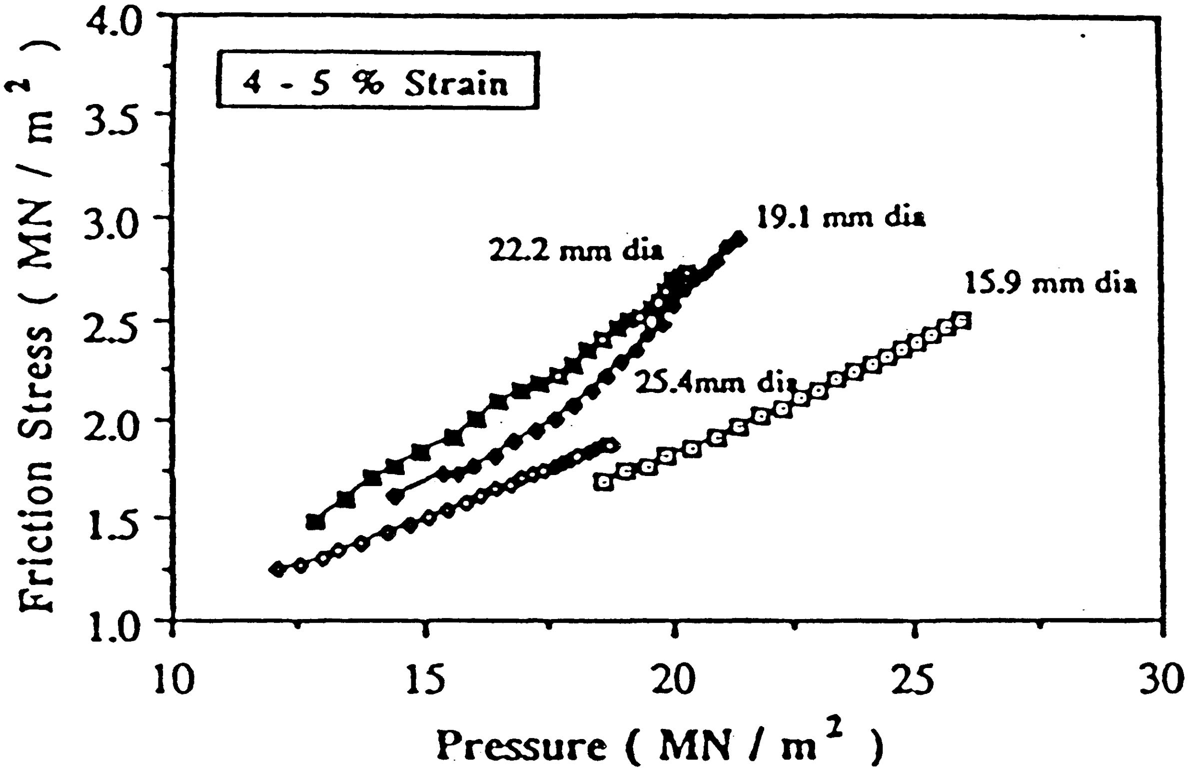

Figure 1.12 The friction stress is shown to increase with increasing contact pressure for an AKDQ sheet steel studied by Wilson (29).

2.0 EXPERIMENTAL DESIGN

The purpose of this study is to gain an understanding of the fundamental relationship between strain rate and die geometry on the frictional behavior of electrogalvanized sheet steels. The work presented here expands previous research done by the Advanced Steel Processing and Products Research Center at the Colorado School of Mines (2,3,41-43) and other work reported in literature (1,12,29,38,44,45). The current research utilizes the Colorado School of Mines bending under tension friction test system modified to accommodate different size roller dies. The reasoning behind the die sizes selected is two fold. First, the four diameters selected represent the typical range of cylindrical geometries found in stamping operations from the 6.35 mm diameter (*i.e.* a draw bead) to the 50.8 mm diameter (*i.e.* a relative flat surface) rollers. Second, the radius of the die influences the contact pressure at the sheet - tool interface and also determines the magnitude of the strain induced in the sheet steel substrate.

The work presented in this thesis examines a commercially produced electrogalvanized coated sheet steel and a cold rolled sheet steel substrate. Both materials were from the same commercially produced coil, thus any base steel properties such as chemical composition and mechanical properties are the same allowing the true influence of the electrogalvanized coating to be determined. The coated and bare sheet steels were selected because they are considered state of the art for current aluminum killed drawing quality (AKDQ) product.

3.0 EXPERIMENTAL PROCEDURE

3.1 Material Selection

The material for this study consisted of 0.76 mm thick aluminum-killed drawing-quality (AKDQ) cold rolled sheet steel and an electrogalvanized AKDQ sheet steel with a coating weight of 60 g/m^2 on both sides of the sheet. Both the uncoated sheet steel and the electrogalvanized sheet steel were obtained from the same coil. This is significant in that variations in mechanical properties between the two materials are minimized. The ladle chemistry for the substrate as supplied by the manufacture is shown in Table 3.1. This material is typical for an AKDQ sheet steel product (46). For the present study, the electrogalvanized sheet steel is referred to as EG4 because it is the fourth commercially produced electrogalvanized sheet material studied in the ASPPRC friction program. The cold rolled sheet steel will be referred to as EG4 substrate.

3.2 Bending Under Tension Friction Testing

All friction tests were conducted using the Colorado School of Mines bending under tension test fixture. The current system, shown schematically in Figure 3.1, was developed by Vallance (2) and modified by Wenzloff (3) to accommodate 305 mm (12 in.) long specimens and to control back force with a servo controlled system. The test system has provisions which allow both the die geometry (roller radius) and strain rate (sliding velocity) to be varied. The roller system consists of cylindrical rollers supported by ball bearings

Table 3.1 Ladle chemistry of the sheet steel.

Alloy	C	Mn	P	S	Si	Cu	Al	N	Ni	Cb	Mo	V
Wt. %	0.043	0.200	0.017	0.007	0.010	0.024	0.029	0.005	0.009	0.003	0.005	0.002

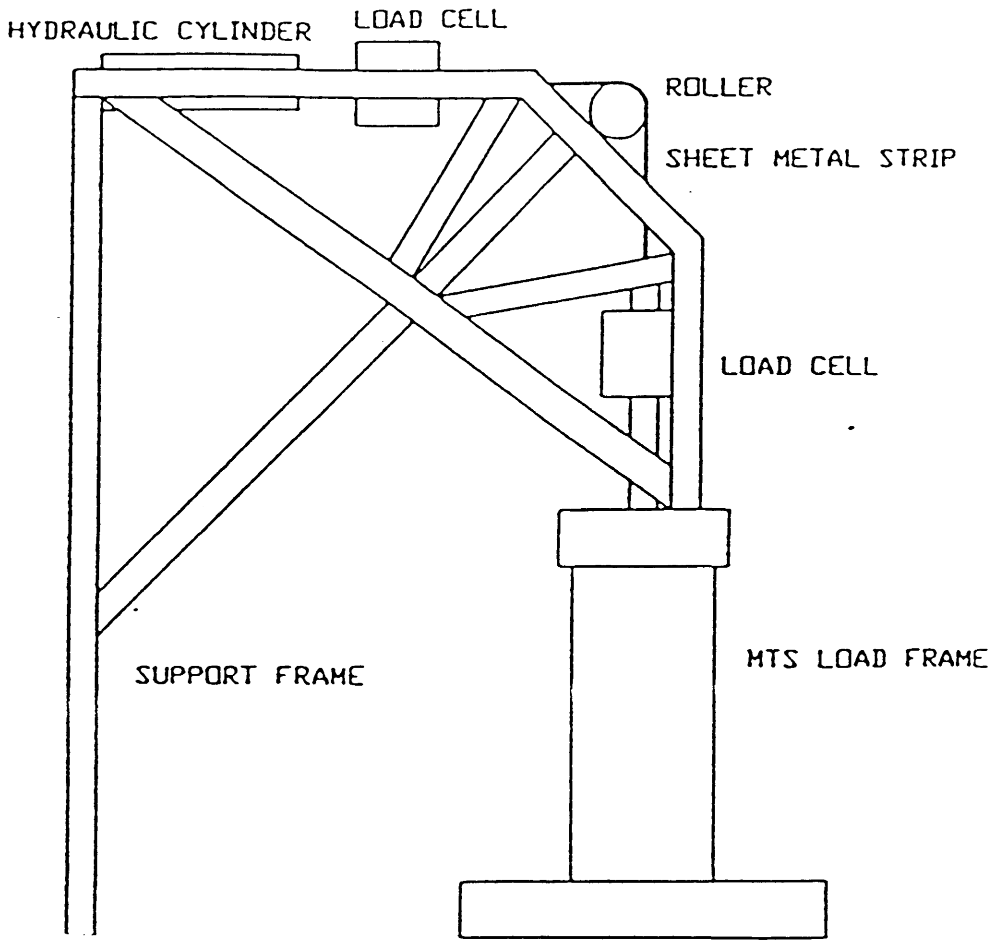

Figure 3.1 Schematic representation of the bending under tension friction test apparatus in use at CSM (2)

mounted in pillow blocks. In this study the system was modified to accommodate rollers with radii between 6.35 and 50.8 mm. The larger rollers (25.4 and 50.8 mm diameters) are supported only by the bearings while the smaller rollers (6.35 and 12.7 mm diameters) are further supported over the entire length by rigid steel backing blocks. The sliding speed is controlled through the MTS Model 458 electronics package. The system is equipped with two servo-controlled hydraulic rams. One actuator produces the desired back force while the second actuator is used to displace the strip at a fixed velocity over the roller (2). By using closed loop testing with servo-hydraulics, precise control of the test parameters is maintained through the duration of the test.

All tests were preformed under the following conditions:

- servo - controlled constant back force (1200 - 5800 N)
- hardened (60 HRC) A2 tool steel rolls with average R_a values of $0.23\mu m \pm 0.025\mu m$ ($9\mu in \pm 1\mu in$)
- samples cleaned with mineral spirits and Kimwipes®, to remove mill oil and debris
- Texaco Almag oil lubrication
- vertical drip method developed by Wenzloff *et al.* (18) to remove excess oil
- test strip geometry of 50.8 mm (2.0 in.) wide 305 mm (12.0 in.) long with the long dimension parallel to the rolling direction
- strip displacement parallel to rolling direction
- test side corresponding to the outside of the coil
- sample displacement of 127 mm (5.0 in.) relative to the roller

3.2.1 Cleaning and Lubrication of the Sample and Die

Prior to each test both the sheet steel sample and tool steel roller were cleaned and lubricated. The procedure for cleaning was adapted from Wenzloff *et al.* (18). Strip cleaning and lubrication consisted of three steps. The residual mill oil and debris was removed from the strip surface with mineral spirits and a Kimwipe®. The strip was allowed to dry before the application of the lubricant. The lubricant, Texaco Almag oil (product code: 01564), was generously applied with a brush and was hung vertically for 300 s, to allow excess lubricant to run off.

The rollers were cleaned and lubricated using a procedure similar to that used for the strips. The roller surface was wiped clean with mineral spirits and lubricated by wiping with the Texaco Almag oil. The excess oil is allowed to accumulate at the bottom of the roller.

3.2.2 Data Collection With the Bending Under Tension Friction Test

The coefficient of friction for each set of conditions (material, speed, and roller diameter) was determined by the bending under tension friction test with constant back force as described in Section 1.2. The bending force for material on the 50.8 mm, 25.4 mm and 12.7 mm rollers was measured with free roller tests while the extrapolation method of Davies and Stewart (19) was used to determine the bending force for the material on the 6.35 mm diameter roller. The friction coefficients for the EG4 and EG4 substrate were calculated with Equation 1.6 with a wrap angle of 90° or $\pi/2$ radians.

3.3 Material Characterization Techniques

3.3.1 Crystallographic Texture Analysis

The crystallographic texture of the electrogalvanized coating was studied with a Rigaku rotating anode x-ray diffractometer. Diffraction patterns were generated over a range of 10 to 90 degrees 2θ using the reflection technique (3,4). As a result of the test method, only planes which were parallel to the coating surface contributed to the measured peak intensities. The Rigaku system employed a filtered copper x-ray tube which produced monochromatic radiation with a wavelength of 0.15418 nm.

A zinc powder diffraction pattern was produced, normalized, and compared to the Hanawalt index for pure zinc. The results of this comparison are presented in Table 3.2. As indicated in Table 3.2, the Hanawalt Index and the normalized powder intensities are essentially the same. This test was done to establish the alignment and accuracy of the equipment. The intensities of the random zinc powder were used to normalize the diffraction intensities from the electrogalvanized coating.

The diffraction pattern of the electrogalvanized coating was analyzed using the "percentage of planes technique" developed by Shaffer *et al.* (23,24). This technique compares x-ray reflection peaks in a random powder sample to those of the electrogalvanized sheet surface. Based on the Hanawalt index crystallographic planes are assigned to the measured peaks. The peaks of the electrogalvanized material are normalized and the material

Table 3.2 Diffraction pattern intensities for pure zinc powder and the Hanawalt index for pure zinc.

Orientation to Basal Plane	Characteristic Plane	Relative Intensity	
		Hanawalt Index	Random Powder
0°	(0002)	53	42
36°	$(10\bar{1}3)$	25	23
47°	$(10\bar{1}2)$	28	22
62°	$(11\bar{2}2)$	23	22
65°	$(10\bar{1}1)$	100	100
90°	$(10\bar{1}0)$	40	26
90°	$(11\bar{2}0)$	21	16

is characterized based on the most intense plane. The "percentage of planes technique" is summarized by the following five steps:

1. Identification of the metallurgically significant planes. In the zinc system these are the following seven planes: basal plane (0002); prismatic planes $(10\bar{1}0)$, $(11\bar{2}0)$; and pyramidal planes $(10\bar{1}3)$, $(10\bar{1}2)$, $(10\bar{1}1)$, $(11\bar{2}2)$.
2. Determination of the peak intensities for each of the seven significant planes and identification of the maximum intensity peak.
3. Normalization of each identified peak by the maximum peak intensity within the test.
4. Determination of the relative intensity ratio for each peak by dividing the coating peak intensity by the corresponding peak from the random powder diffraction pattern.
5. Calculation of the percentage value for each plane by summing the relative intensity ratios and then dividing each ratio by the sum of the ratios.

The texture of the electrogalvanized coating is classified by the most dominant plane or planes (*i.e.* prismatic, low angle pyramidal with a slight basal plane orientation, *etc.*) as determined by the percentage of planes technique. Figure 3.2 shows schematically the seven metallurgically significant planes and the angle of each from the basal plane (16). Texture results for this study will be presented in the same manner, that of frequency as a function of zinc crystallographic plane.

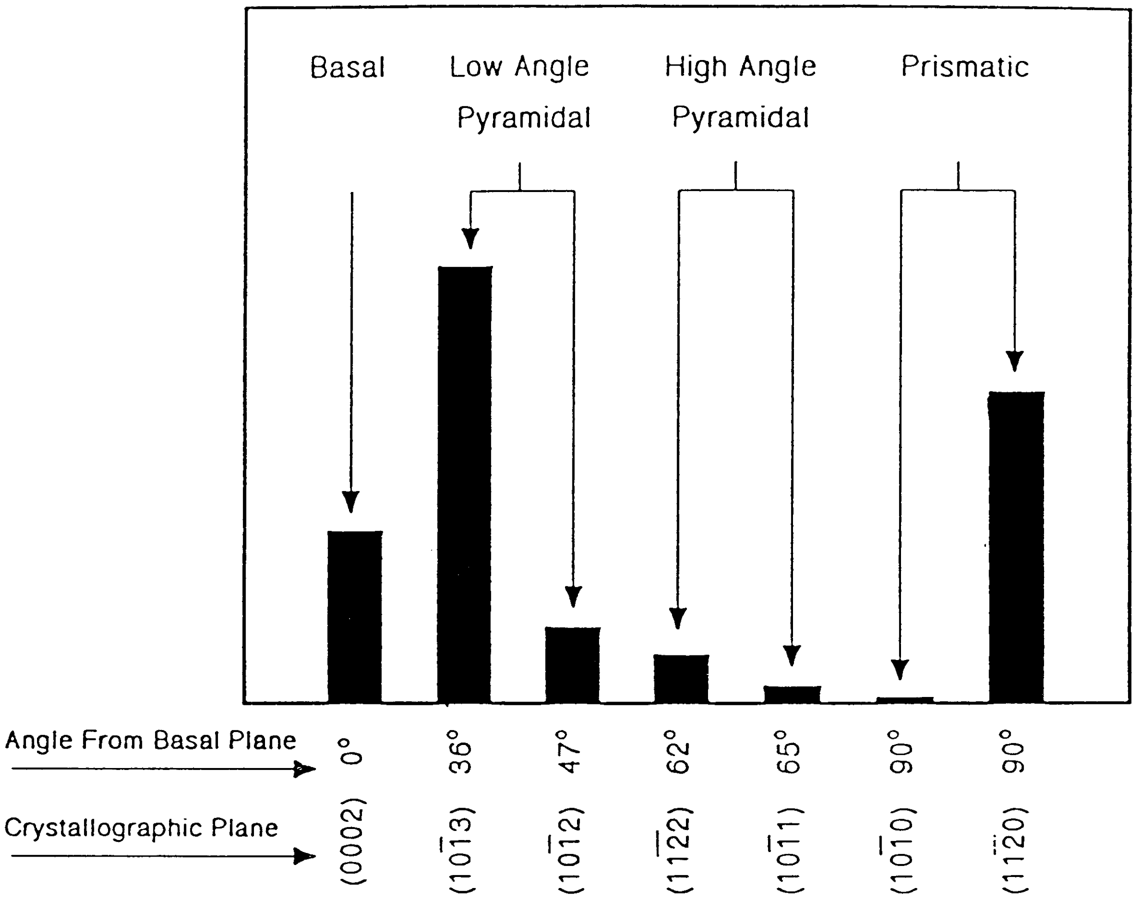

Figure 3.2 The seven metallurgically significant planes in the zinc crystal system. The height of the bars represent the relative intensity of each plane.

3.3.2 Roughness Testing

Roughness testing was performed on an Alpha-Step 200 profilometer. The Alpha-Step utilizes a diamond stylus and has the following features:

1. A variable stylus force of 0 to 25 milligrams.
2. Diamond stylus radius of 1 μm.
3. RS232 port for data transfer to a computer.
4. Variable trace length of 0 to 10,000 μm.

The direct output of the Alpha-Step 200 includes the average roughness, R_a, of the sample and a plot of the surface height versus trace distance. Profile height versus position data were also recorded with a portable computer-based data acquisition system. The ability to analyze the data by means other than those inherent in the Alpha-Step 200 allows a more detailed analysis of the surface profile.

A spreadsheet based program (47) was used to analyze the height profile data and determine specific roughness parameters. The following roughness parameters were calculated:

1. The arithmetic average peak height R_a, the arithmetic average of all values of the roughness profile of peaks which lie above the mean line.
2. The average roughness R_q, the root mean square of all values of the roughness profile of peaks which lie above the mean line.

3. The maximum roughness R_m, the greatest perpendicular distance between the highest peak and lowest valley.

4. Peak count P_c, the number of peaks within a given trace which rise above a selected reference line.

5. Abbott bearing area ratio curve, a plot of bearing area ratio versus penetration depth.

A 1 μm diamond stylus with a 7 mg load was used for both cold rolled substrate and electrogalvanized specimens. Two traces, end-to-end, each 2000 μm long were made transverse to the rolling direction and added together to obtain a single data set containing 4000 points over a total of surface length of 4000 μm.

3.3.3 Coating Grain Size Determination

In addition to the coating texture and roughness the average grain size of the zinc was determined. The method prescribed by Wenzloff *et al.* (26) was used to classify the grains as either coarse or fine based on a grain structure with an average grain size smaller than 5 μm as fine and those larger than 5 μm as coarse.

3.3.4 Contact Area Analysis Method

Scanning electron microscope (SEM) images were obtained with a Joel JXA-940 Scanning Micro Analyzer. SEM photomicrographs were taken at 50X of each set of test conditions for different calculated contact pressures. The true contact areas were determined by point counting per ASTM E562 (48). The locations studied for contact area analysis were the same for each sample and corresponded to the center of the contact region of the sheet after friction testing.

3.3.5 Mechanical Properties Evaluation

Tensile testing of both the EG4 substrate and EG4 steel sheets were preformed on a screw type Instron test frame. The test specimens were standard ASTM E8 (49) samples; reduced gage sections of 12.7 mm (0.5 in.) wide and 50.8 mm (2 in.) long. From the tensile testing data the yield strengths (σ_y), the ultimate tensile strengths (UTS), and total elongations (ε_T) of both EG4 and the substrate were determined. All tensile testing was performed at room temperature (~25°C) and a constant engineering strain rate of 0.01 m m^{-1} s^{-1}.

4.0 RESULTS

4.1 Material Characterization

The two materials which are the focus of the present study were characterized by a variety of experimental tests. Both the substrate and the electrogalvanized sheet steel were tested to determine the as-received: 1) mechanical properties of the substrate, 2) surface roughness of both the substrate and coated material, 3) crystallographic texture of the electrogalvanized zinc coating, and 4) the grain size of the zinc coating.

4.1.1 Mechanical Properties

Mechanical properties studied, of both the coated and uncoated sheet steel, consisted of tensile strength and total tensile elongation and are summarized in Table 4.1. Note that the yield strength, ultimate tensile strength and total elongation properties are essentially independent of orientation. The results for the uncoated material are an average of six tests in each orientation while the coated material results are an average of three tests in each orientation.

4.1.2 Coating and Substrate Surface Roughness

The surface roughness values for the as-received materials are summarized in Table 4.2 and include results for traces transverse to the rolling direction. The results in Table 4.2, which include the arithmetic average roughness (R_a), the maximum roughness depth (R_m), and the average root mean square roughness (R_q) values indicate that both the substrate and coated

Table 4.1 Tensile properties for the EG4 sheet steel in both the coated and uncoated condition.

Orientation of Tested Material	Yield Strength (MPa)	Ultimate Tensile Strength (MPa)	Percent Elongation
Substrate Parallel to Rolling Direction	152	315	44
Substrate Transverse to Rolling Direction	152	315	46
EG4 Parallel to Rolling Direction	175	308	44
EG4 Transverse to Rolling Direction	182	308	49

Table 4.2 Surface roughness values for both EG4 and EG4 substrate and the other three commercially coated samples previously tested.

Roughness Parameter	EG4 Substrate (Sheet Steel)	EG4 (Electrogalvanized Coated)	EG1 (50)	EG2 (50)	EG3 (50)
R_a (μm)	0.9	0.8	0.9	0.8	1.2
R_m (μm)	5.9	5.9	NT	NT	NT
R_q (μm)	1.1	1.0	NT	NT	NT

NT = Not Tested

material have similar surface roughnesses. This implies that variations to the micro roughness due to the presence of the coating are not detectable by the light load stylus measurements. Also in Table 4.2 are R_a values for EG1, EG2 and EG3, commercially coated electrogalvanized materials with coating weights similar to EG4, for comparison (27,41,50). It is observed that the magnitude of the surface roughness value of the EG4 material is similar to those of the other commercially produced electrogalvanized materials previously studied at CSM.

4.1.3 Crystallographic Texture of the Electrogalvanized Zinc Coating

The peak intensities for the powder and sheet samples were normalized by the intensities of the corresponding maximum peaks. The analyzed crystallographic data were then presented in a bar chart in the same order as Figure 3.2. The frequency of each of the seven metallurgically significant planes in the zinc crystal is shown in Figure 4.1. From Figure 4.1 the most prominent plane observed is the $(10\bar{1}3)$ plane. The dominance of the $(10\bar{1}3)$ plane indicates that the coating on the EG4 material has a low angle pyramidal texture. For completeness, the texture of EG4 was compared to the other commercially produced electrogalvanized coated sheet steels. Both EG1 and EG4 are classified as low angle pyramidal; the EG2 has a combination texture comprised of both low and high angle pyramidal; and the EG3 is a combination of prismatic and low angle pyramidal (16,17).

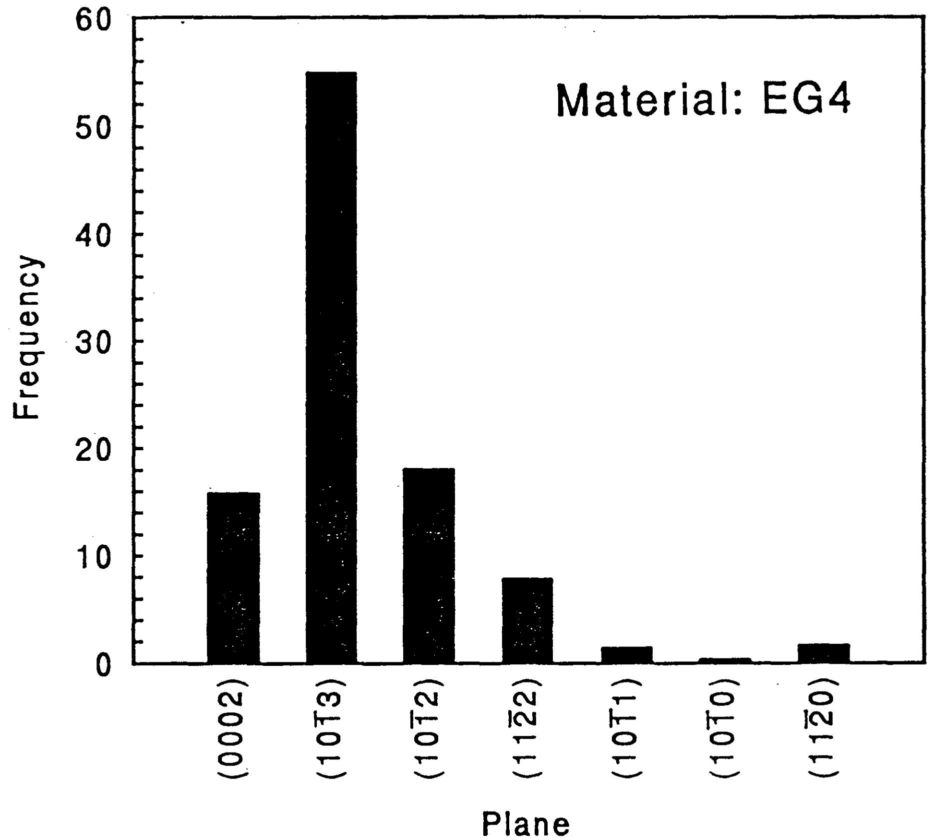

Figure 4.1 Histogram of the crystallographic texture for the EG4 electrogalvanized coated sheet steel. The (10$\bar{1}$3) plane is the dominate plane indicating that the coating has a low angle pyramidal texture.

4.1.4 Coating Grain Size Analysis

From photomicrographs such as those shown in Figure 4.2, the grain size of the electrogalvanized zinc coating can be classified. Based on the classification system developed by Wenzloff (3) the coating of EG4 is categorized as coarse with a typical grain size of approximately 22 μm.

4.2 Friction Testing

4.2.1 Bending Force Data

The measured bending forces for the 12.7, 25.4 and 50.8 mm roller diameters are summarized in Table 4.3. The reported values are an average of at least three tests for each roller diameter. The back forces were selected to cover the range of back forces experienced in the fixed roller tests. The free roller tests indicated that the bending force, F_b generally decreased with increasing back force but the difference between the average and each measured bending force is within the electrical noise of the data acquisition system and does not affect the calculated coefficient of friction. Note that the bending force increases as roller diameter decreases owing to the high strain imposed at the smaller radii.

The bending force for the 6.35 mm diameter roller was determined with the intercept method of Davies and Stewart (19) due to flexure of the roller under loads below the bending force. Figure 1.7 illustrates this method of determining the bending force. The bending force for the 6.35 mm diameter roller was determined to be 1880 N as shown in Figure 4.3 and Table 4.3.

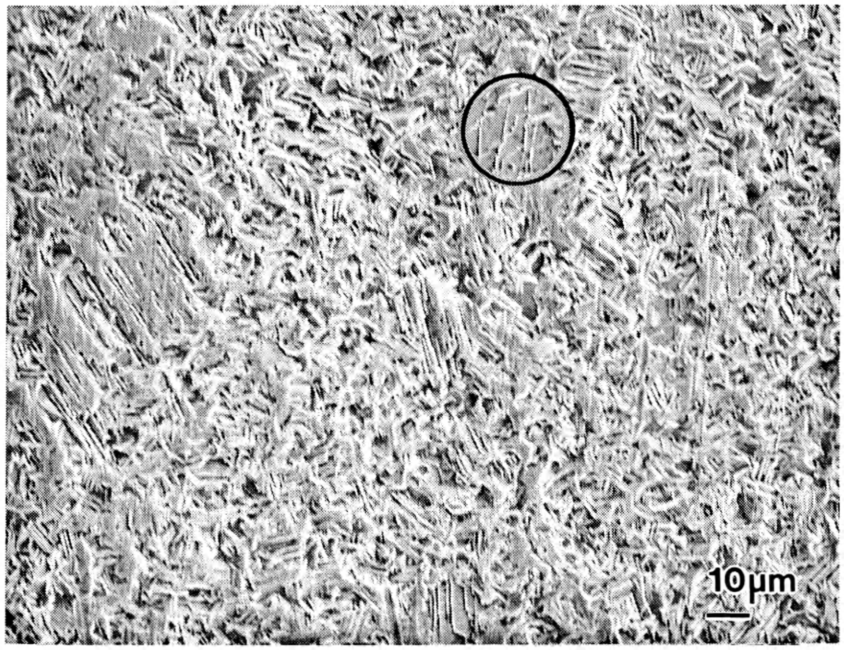

Figure 4.2 Undeformed (*i.e.* not tested) zinc surface. A single zinc grain is circled. The grain size is considered coarse because it is larger than 5μm. SEM micrograph.

Table 4.3 Bending forces determined using free roller tests for the 50.8 mm, 25.4 mm and 12.7 mm diameter roller and the intercept method for the 6.35 mm roller.

Roller Diameter (mm)	Measured Bending Force (N)
50.8	102
25.4	245
12.7	676
6.35	1880

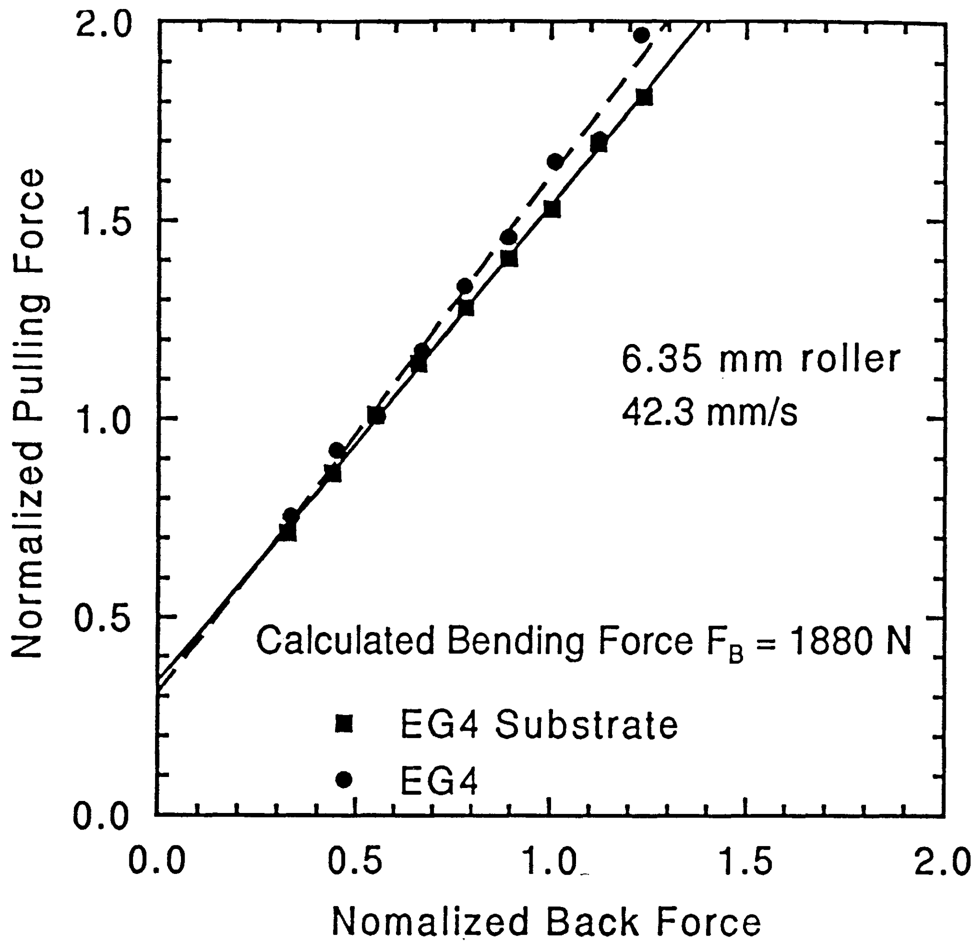

Figure 4.3 The method of Davies and Stewart (19) as used to determine the bending force for the 6.35 mm diameter roller. The bending force, F_b, was determined form the plot to be 1880 N.

4.2.2 Measured Coefficients of Friction

Bending under tension friction test force data were obtained for each set of test parameters: material, test speed and roller diameter. Figure 4.4 shows a typical normalized adjusted pulling force versus normalized back force plot with data for the 50.8 mm diameter roller at a displacement rate of 4.23 mm/s. Note the linearity of the best fit line for the data obtained. The high degree of linearity is typical of all twelve roller diameter - displacement rate combinations considered in this study. The normalized adjusted pulling force versus normalized back force data plots for all test parameter combinations can be found in Appendix A. From the linearity it appears that μ is independent of pressure.

The coefficients of friction for both EG4 and EG4 substrate are summarized in Table 4.4. The value of each friction coefficient, μ, was determined with Equation 1.6. The slope of the normalized adjusted pulling force versus normalized back force as determined by a best fit linear least squares line was used as the argument of the logarithmic term. The measured values of the friction coefficient ranged from 0.16 to 0.23 for EG4 substrate and from 0.19 to 0.55 for EG4.

4.2.3 Special Consideration Concerning the 6.35 mm Roller Tests

The 6.35 mm roller tests posed a challenge as compared to the three larger diameter experiments. With a decrease in roller diameter the pressure at the interface increased such that at the 6.35 mm diameter roller the pressure is eight times greater than the pressure experienced when using the 50.8 mm diameter roller assuming the applied forces are the same. As discussed in Section 1.3 the lubrication regime is speed and pressure sensitive and

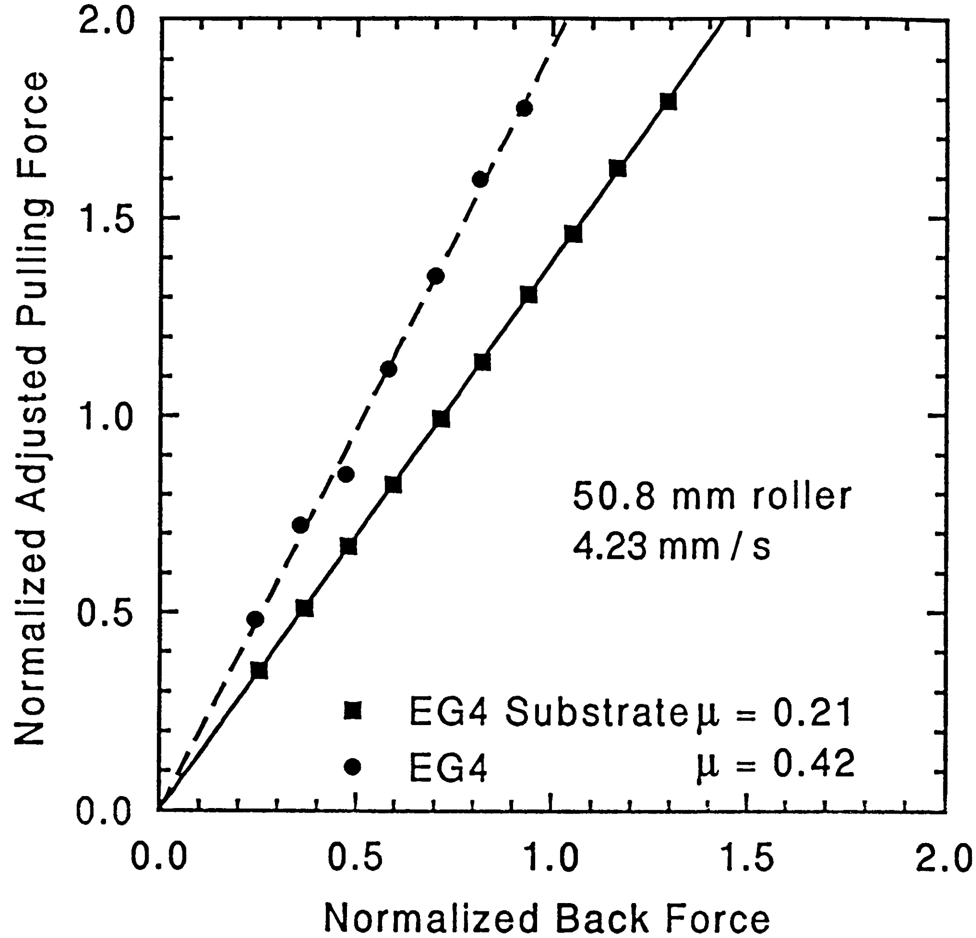

Figure 4.4 Normalized adjusted pulling force versus normalized back force plot for the 50.8 mm diameter roller at 4.23 mm/s. The linearity of the best fit line is typical of the other eleven test sets.

Table 4.4 Friction coefficients for EG4 and EG4 substrate at various sliding speeds and roller diameters.

	Friction Coefficient: μ					
	42.3 mm/s		4.23 mm/s		0.423 mm/s	
Roller Diameter	EG4 Sub	EG4	EG4 Sub	EG4	EG4 Sub	EG4
50.8 mm	0.20	0.24	0.21	0.42	0.23	0.55
25.4 mm	0.17	0.19	0.19	0.43	0.22	0.39
12.7 mm	0.17	0.22	0.19	0.46	0.21	0.49
6.35 mm*	0.17	0.20	0.18	0.21	0.16	0.38

* Determined using a calculated bending force.

the decreased speed combined with increased pressure resulted in coating deformation that was unique to 6.35 mm diameter roller tests at a displacement rate of 0.423 mm/s. This deformation mode consisted of cracking, peeling and flaking of the coating on EG4 and the degree of coating failure increased with increasing contact pressure. The resulting EG4 coating surface is shown in Figure 4.5. The three samples in Figure 4.5 show the progression of coating damage with increasing contact pressure. The pressures ranged from 2.1 to 7.8 MPa (305 to 1130 psi).

4.3 Contact Area Analysis

In order to study the effects of contact pressure and sliding speed on the frictional behavior of EG4 true plastic contact area measurements were made after friction testing. The effect of contact pressure on contact area was determined by fixing the applied forces and changing the roller diameter. The resultant surfaces obtained from testing on the four different roller diameters are shown in Figure 4.6. These samples all experienced the same applied back force (4450 N), and sliding velocity (4.23 mm/s). From Figure 4.6 the true contact area was calculated based on the observed amount of asperity deformation. The calculated contact area increased as the roller radius decreased, from 47% contact area on the 50.8 mm diameter roller to 68% contact area on the 6.35 mm diameter roller. Note that at a constant back force the contact pressure increased with a decrease in roll radius.

The effect of sliding speed on the true contact area at a constant contact pressure was determined in a series of tests. This testing was performed on the 25.4 mm diameter roller with an applied back force of 4450N. The results are presented in Figure 4.7 in the form of a plot of percent deformed region versus sliding velocity. As shown in Figure 4.7, with in the indicated data band, the contact area increases with decreasing sliding speed.

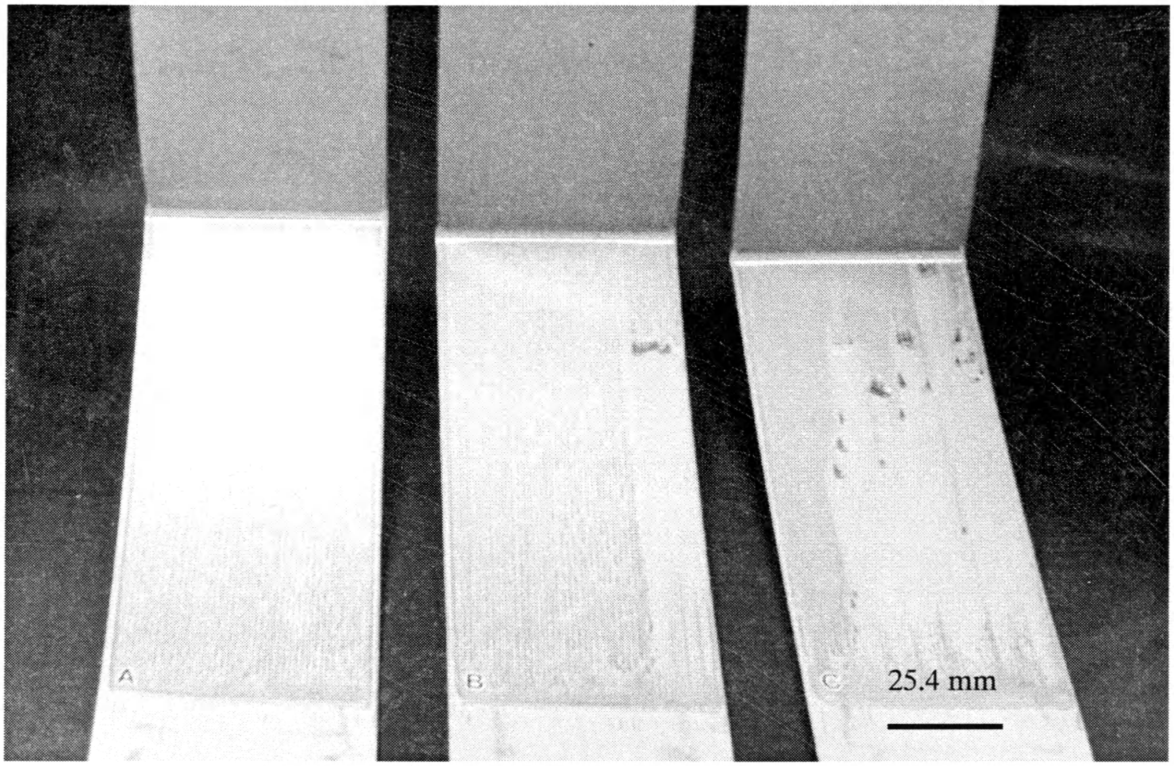

Figure 4.5 EG4 strips that show indications of zinc flaking off at different contact pressures. A) low pressure B) medium pressure C) high pressure. Photomacrograph.

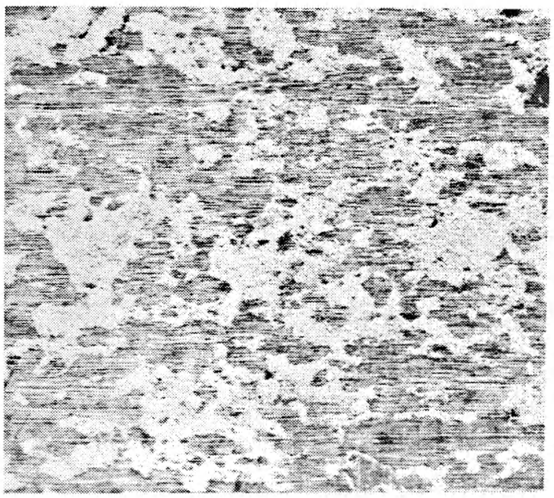

50.8 mm diameter roller
Contact area = 47%

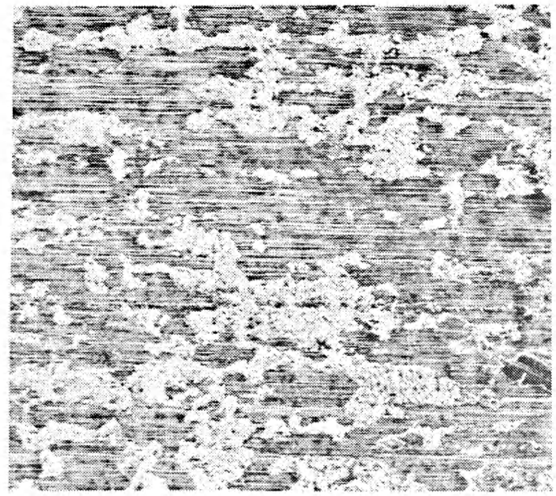

25.4 mm diameter roller
Contact area = 58%

12.7 mm diameter roller
Contact area = 59%

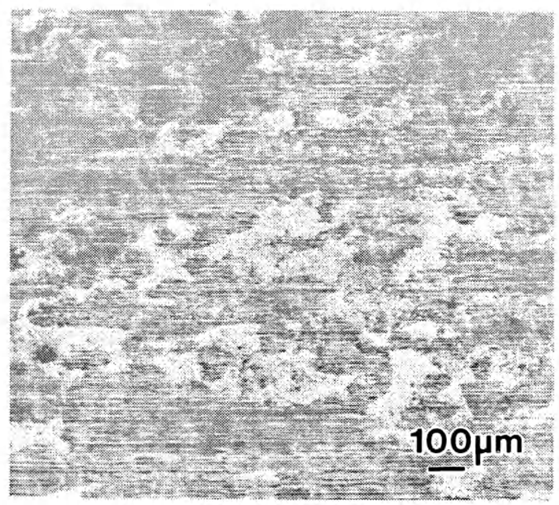

6.35 mm diameter roller
Contact area = 68%

Figure 4.6 Amount of contact area resulting form different roller diameters. All four samples were tested with applied back force of 4450 N at 4.23 mm/s. Photomacrographs.

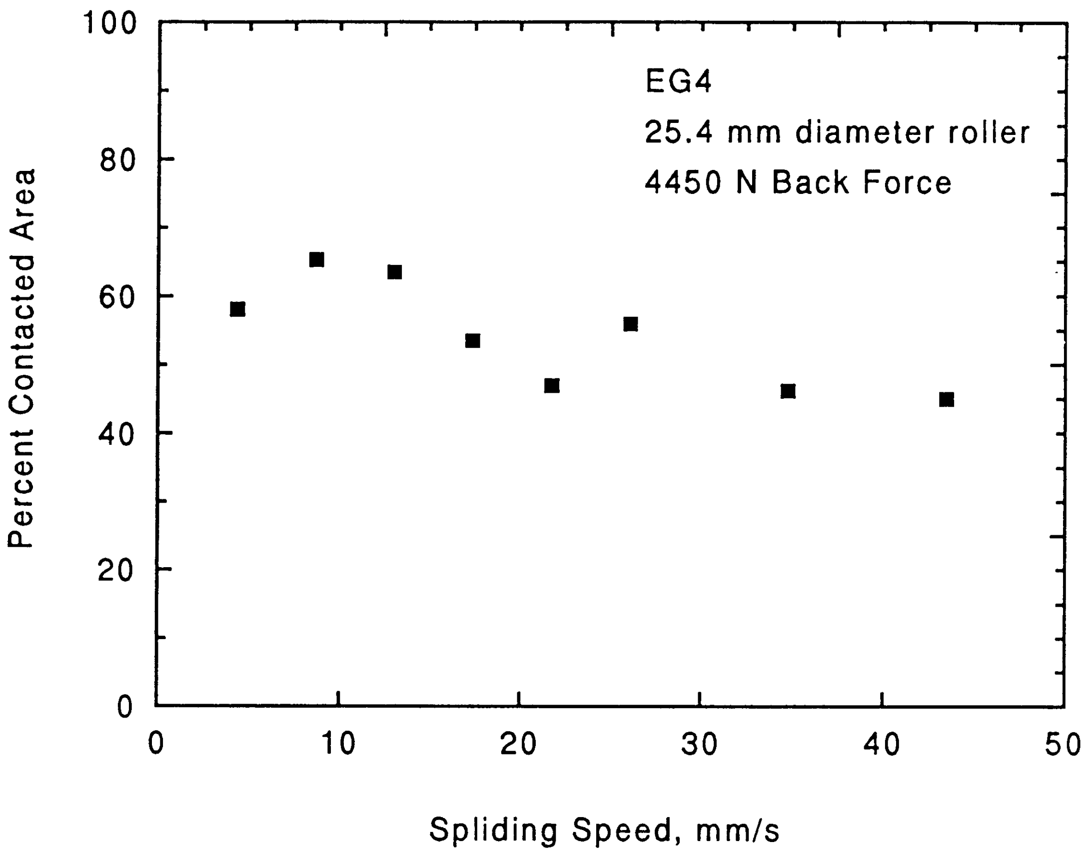

Figure 4.7 Plot of contact area as a function of sliding speed for the 25.4 mm diameter roller. Note that the measured contact area decreases as the sliding speed increases.

5.0 DISCUSSION

The results presented in the previous section indicate that both die geometry and relative sliding speed affect the measured friction coefficient on electrogalvanized sheet steel. In this discussion the accuracy of the reported values of μ is addressed based on a Kline - McClintock second power law analysis of the friction equation along with a short analysis of the repeatability of results obtained on uncoated cold rolled sheet steel materials. Also in this section, the measured coefficients of friction are interpreted with respect to the test parameters. The current friction results obtained from the EG4 material are compared to friction data on the other three commercially produced electrogalvanized materials studied previously (2,50) and the results are tabulated in Table 5.1.

5.1 Sensitivity Analysis of Reported Coefficients of Friction

The bending under tension friction test has been extensively used to determine the coefficient of friction, μ, for a variety of sheet steels, both coated and uncoated. The accuracy of the testing and reporting methods has not been quantitatively analyzed. The analysis presented in this section addresses the issue of the sensitivity of calculated μ-values determined by the bending under tension friction test to variations in the experimental measurements used to calculate μ. This sensitivity analysis determines an uncertainty value which is similar to the experimental error associated with a given value of μ.

To determine an overall uncertainty in μ, an understanding of the sensitivity of the friction equation to each individual component must be determined. Once the sensitivity of

Table 5.1 Summary of results for the four electrogalvanized sheet steel materials tested at CSM (50). Test conditions consisted of 42.3 mm/s sliding speed and 25.4 mm diameter roller.

Material	R_a, μm	Texture	μ	Reference
EG1	0.6	LAP/Basal	0.20	(50)
EG2	0.8	LAP/HAP	0.19	(50)
EG3	1.0	Prismatic/HAP	0.14	(50)
EG4	0.8	LAP	0.19	--

each experimental component is known then the uncertainty (or experimental error) for the reported value of μ can be given with a degree of mathematical precision.

5.1.1 The Friction Equation

The equation used to obtain the friction coefficient in the CSM bending under tension friction test can be derived based on either energy or force considerations (2,13) and incorporates the sheet thickness, roll radius, the force to bend the strip, the back tension force and the front pulling force. The friction coefficient is determined from Equation 1.6 and for the completeness in the presentation of this section it is shown again below.

$$\mu = \frac{2}{\pi}\left(\frac{r+0.5t}{r}\right)\ln\left(\frac{F_1-F_B}{F_2}\right) \qquad [5.1]$$

where: r = roll radius

t = sheet thickness

F_1 = pulling force

F_2 = back force

F_B = bending force

The values of the F_1 and F_2 are forces measured directly during the test using calibrated load cells. The experimental error or uncertainty of these force values directly relates to the accuracy of the load cells. F_B is obtained from the difference between the front and back tension forces obtained in the free roller test. The uncertainty of the bending force is the sum of the uncertainties of the front and back tension load cells. The radius, r, and the sheet thickness, t, are geometric values and the uncertainty of these values are related to the micrometer used for measurement.

5.1.2 Kline - McClintock Second Power Law

An estimate of uncertainty in a calculated value can be obtained from the Kline - McClintock second power law (51). The contribution of the uncertainty of each variable to the total uncertainty of a calculated value can be obtained via a geometrical averaging process. For the specific case under consideration, the uncertainty in the friction coefficient, U_μ, is given by the following equation:

$$U_\mu = \pm\left[\left(\frac{\partial\mu}{\partial F_1}U_{F_1}\right)^2+\left(\frac{\partial\mu}{\partial F_B}U_{F_B}\right)^2+\left(\frac{\partial\mu}{\partial F_2}U_{F_2}\right)^2+\left(\frac{\partial\mu}{\partial r}U_r\right)^2+\left(\frac{\partial\mu}{\partial t}U_t\right)^2\right]^{\frac{1}{2}} \qquad [5.2]$$

where: U_{F_1} is the uncertainty in the value of F_1

U_{F_B} is the uncertainty in the value of F_B

U_{F_2} is the uncertainty in the value of F_2

U_r is the uncertainty in the value of the roll radius r

U_t is the uncertainty in the value of the sheet thickness, t

The partial derivatives in Equation 5.2 are obtained from Equation 5.1 by taking the partial derivative of μ with respect to each desired variable. For the bending under tension test the geometric variables are t, the sheet thickness and r, the roll radius and the force variables are F_1 the pulling force, F_2 the back force and F_B the bending force. Equation 5.3 is an example of the partial derivative of μ with respect to r.

$$U_\mu = \frac{2}{\pi}\left(\frac{r + 0.5r}{r}\right)\ln\left(\frac{F_1 - F_B}{F_2}\right)\left\langle \left[\frac{1}{F_1 - F_B}\frac{1}{\ln\left(\frac{F_1 - F_B}{F_2}\right)}\right]^2 U_{F_1}^{\ 2} \right.$$

$$+\left[\frac{-1}{F_1 - F_B}\frac{1}{\ln\left(\frac{F_1 - F_B}{F_2}\right)}\right]^2 U_{F_B}^{\ 2}$$

$$+\left[\frac{-1}{F_2}\frac{1}{\ln\left(\frac{F_1 - F_B}{F_2}\right)}\right]^2 U_{F_2}^{\ 2} \qquad [5.4]$$

$$+\left[\frac{-0.5t}{r^2}\frac{1}{\left(\frac{r + 0.5t}{r}\right)}\right]^2 U_r^2$$

$$\left. +\left[\frac{0.5}{r}\frac{1}{\left(\frac{r + 0.5r}{r}\right)}\right]^2 U_t^2 \right\rangle^{\frac{1}{2}}$$

The other partial derivatives are determined in a similar fashion. Substituting the five partial derivatives into Equation 5.2 yields:

$$\mu = \frac{2}{\pi}\left(\frac{r + 0.5t}{r}\right)\ln\left(\frac{F_1 - F_B}{F_2}\right)$$

$$\frac{\partial\mu}{\partial r} = \frac{2}{\pi}\ln\left(\frac{F_1 - F_B}{F_2}\right)\left[\frac{1}{r} - \frac{r + 0.5t}{r^2}\right]$$

$$\frac{\partial\mu}{\partial r} = \frac{2}{\pi}\ln\left(\frac{F_1 - F_B}{F_2}\right)\left[\frac{r - r - 0.5t}{r^2}\right] \qquad [5.3]$$

$$\frac{\partial\mu}{\partial r} = \frac{2}{\pi}\ln\left(\frac{F_1 - F_B}{F_2}\right)\left[\frac{-0.5t}{r^2}\right]$$

Equation 5.4 provides a direct value of the uncertainty of μ as a function of the uncertainties of the five (3 force and 2 geometric) parameters which are used in its computation. Each term inside the braces of Equation 5.4 is a measure of the contribution that the specific parameter makes to the overall uncertainty in the value of μ which is reported. This analysis is based on English units due to the fact that the test system is calibrated in these units.

5.1.3 Application of the Kline - McClintock Second Power Law to Experimental Bending Under Tension Test Results

Friction coefficients obtained with the bending under tension friction test historically have been reported as a single value, μ (2,3,13). The Kline - McClintock second power law enables the value of the friction coefficient to be reported with a specific value of uncertainty. To illustrate the predicted uncertainty in μ, an example calculation is presented below.

A typical set of experimental test values for a bending under tension test is given in Table 5.2. To obtain the overall uncertainty in μ, measurement uncertainties in each of the individual parameters are required. In Tables 5.3 and 5.4, reasonable uncertainty values for the force and geometric measurements are presented along with the relative contribution of each parameter's uncertainty to the total uncertainty in μ. The relative contribution is equivalent to the parameter inside each set of parentheses in Equation 5.2. The selected uncertainties span the range of realistic experimental measurements. The relative contribution of each variable to the total uncertainty in μ is obtained by multiplying the uncertainty (column 1 in Tables 5.3 and 5.4) by the partial derivative value to obtain the values which appear in columns 2 or 3 in Tables 5.3 and 5.4. It should be noted that the uncertainty in the

Table 5.2 Typical values for measured variables in the bending under tension friction test.

Front Force (lbs.)	Back Force (lbs.)	Bending Force (lbs.)	Roll Radius (in.)	Sheet Thickness (in.)
1500	1000	50	0.50	0.030

Table 5.3 Relative contribution to the total uncertainty of μ from the force parameters.

Force Uncertainty (U_F)	$\partial\mu/\partial F_1\, U_{F1}$ or $\frac{1}{2}\partial\mu/\partial F_B\, U_{FB}$	$\partial\mu/\partial F_2\, U_{F2}$
3 lbs.	0.0057	0.0081
6 lbs.	0.0111	0.0162
12 lbs.	0.0222	0.0323
24 lbs.	0.0445	0.0646

Table 5.4 Relative contribution to the total uncertainty of μ from the geometric parameters.

Geometric Uncertainty (U_r or U_t)	$\partial\mu/\partial r\, U_r$	$\partial\mu/\partial t\, U_t$
0.0005 in.	0.000029	0.0018
0.001 in.	0.000058	0.0036
0.005 in.	0.000291	0.0179
0.010 in.	0.000583	0.0357
0.050 in.	0.002913	0.4455

bending force, U_{FB}, is twice the uncertainty in the front tension force or the back tension force, since the bending force value is determined by the difference of the two force measurements during a free roller test.

From Tables 5.3 and 5.4, it is observed that the dominant factors in the total uncertainty in the friction coefficient are due to the force measurements. The radius parameter does not significantly contribute to the total uncertainty until an uncertainty value of ± 0.050 in. (± 1.270 mm) is reached. Likewise, the sheet thickness parameter does not significantly contribute to the total uncertainty until an uncertainty value of ± 0.001 in. (± 0.0254 mm) is reached. Dimensional precision greater than these uncertainty values is easily obtainable using standard measurement equipment for the geometric parameters.

The uncertainty levels in the force measurements reflect the sensitivities of both the load cells and the corresponding data acquisition system. Repeatable measurements in force of ± 3 lbs. or $U_F = 6$ lbs. (± 13.3 N or $U_F = 26.6$ N) are normally obtained in the bending under tension friction test at CSM.

The relationships of $\partial\mu$ to the back force for the four uncertainties, U_F, summarized in Table 5.3 are shown in Figure 5.1. From this plot it can be seen that $\partial\mu$ is less than 0.01 when $U_F = 13.3$ N for all back forces and $U_F = 26.6$ N for back forces greater than 15835 N. The values in Figure 5.1 are for constant values of U_r and $U_t = 0.0127$ mm.

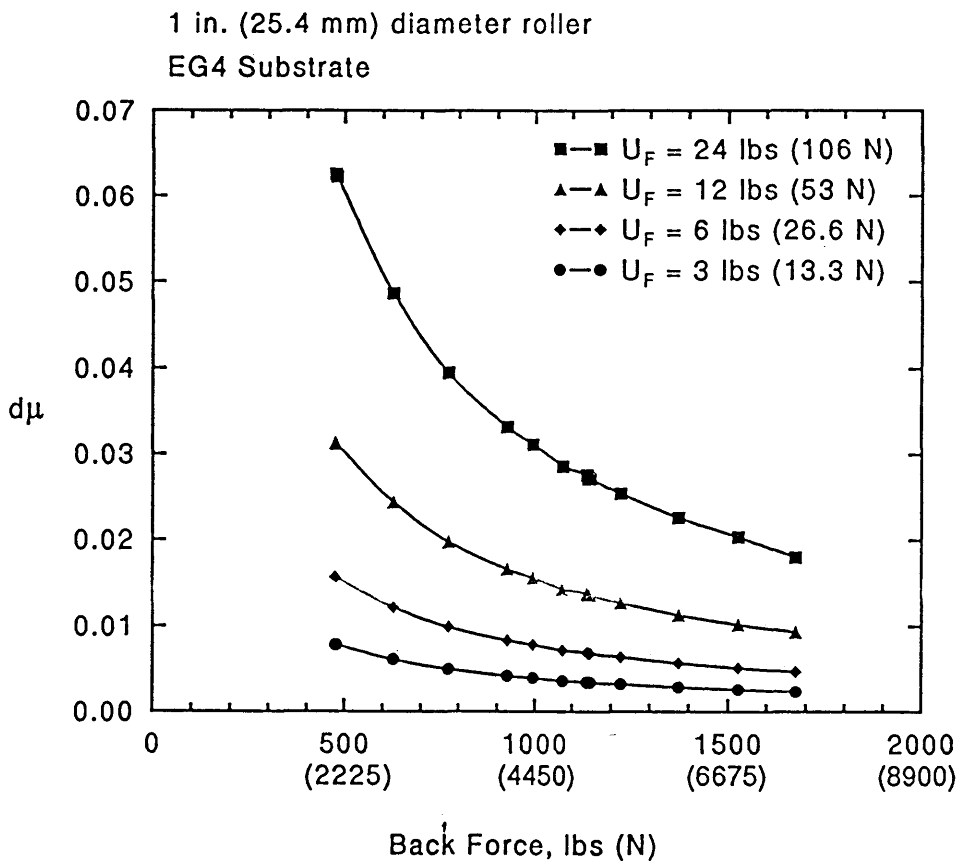

Figure 5.1 The relationship of $\partial\mu$ to the back force for four uncertainties in force, U_F. $\partial\mu$ is less than 0.01 when U_F = 6 lbs (26.6 N) for back forces greater than 800 lbs (3560 N).

5.1.4 Implication of the Kline - McClintock Second Power Law Analysis to Measured Values of the Friction Coefficient

The results of the sensitivity analysis of the friction coefficient obtained in the bending under tension friction test allows a higher degree of confidence to be placed on reported values for friction coefficients. The friction coefficient can be stated as $\mu \pm U_\mu$ and for the results obtained with the CSM bending under tension test, this implies that quoted μ-values are accurate to at least ± 0.01.

5.2 Repeatability of Measured Friction Coefficients

The issue of repeatability of results obtained with the bending under tension friction test is best addressed by the following example. The example consists of friction testing on two uncoated AKDQ cold rolled sheet steels obtained from different suppliers on a 25.4 mm diameter roller at a displacement rate of 42.3 mm/s. The materials are designated EG2 substrate which was studied by Vallance (2) and Wenzloff (3) and EG4 substrate tested in the as-received condition as outlined in Section 3.2. A direct comparison of friction data obtained on the two uncoated materials is presented in Figure 5.2, a plot of adjusted pulling force versus back tension force. Figure 5.2 indicates that the force data for the two uncoated substrates superimpose to describe a single linear function, and correspondingly the same friction coefficient, 0.17. The equivalency between the friction coefficients on the two uncoated substrates leads to two important observations with respect to bending under tension friction measurements: first, the friction coefficient between uncoated sheet steel and the hardened steel roller lubricated with Texaco Almag oil is 0.17 and is independent of slight

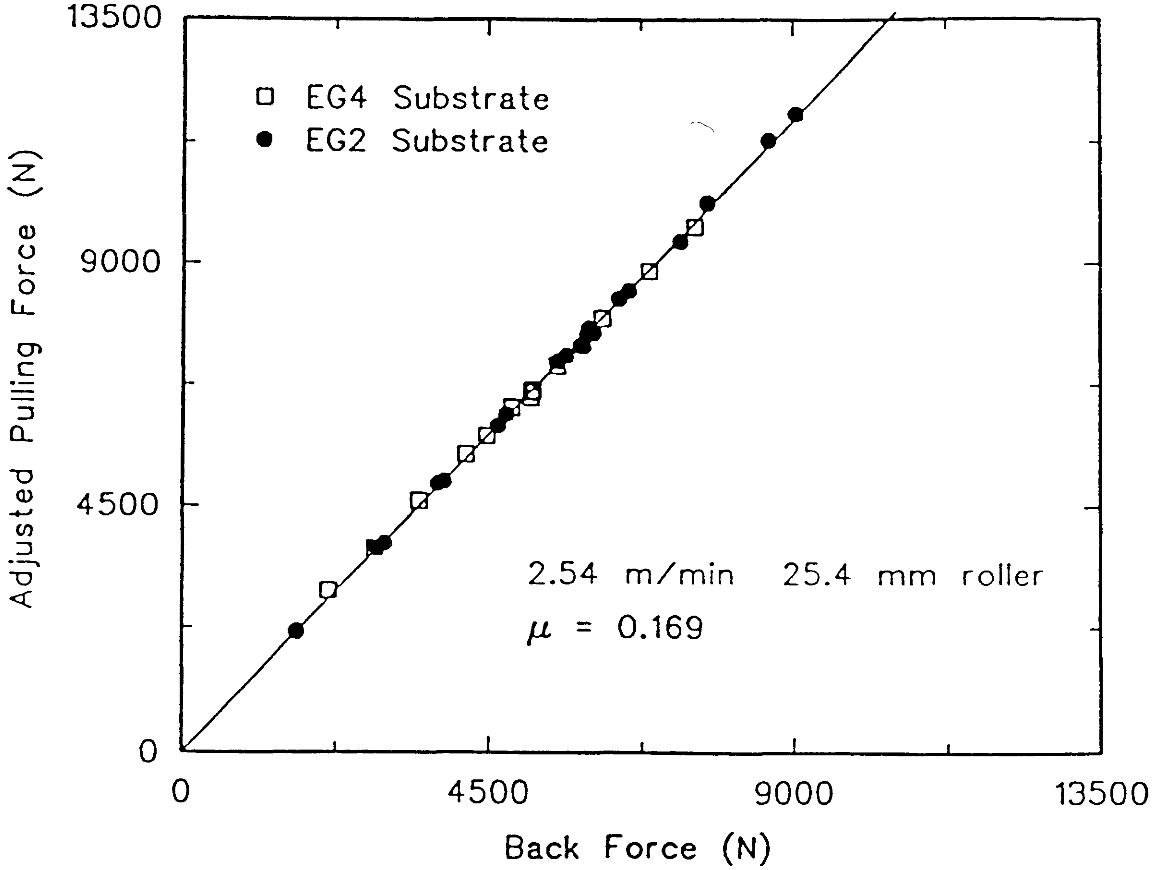

Figure 5.2 Plot of adjusted pulling force verses back force for EG4 substrate and the EG2 cold rolled sheet steel previously tested (3). Note the two sets of data superimpose resulting in a $\mu = 0.17$.

variations in surface roughnesses of both the roller and the sheet; and secondly, friction testing with the equipment at CSM is repeatable. Also, the constant value obtained in two cold rolled AKDQ sheet steels indicates the presence of zinc coatings significantly alters μ and thus measured frictional characteristics are truly a result of the coating.

5.3 Roller Diameter Effects

At a constant test speed, friction coefficients as summarized in Table 4.4 for the EG4 substrate decrease slightly with a decrease in roller diameter. However, the corresponding measurements on the coated EG4 material indicate that at a specific test speed the measured friction coefficients are essentially independent of roller diameter as indicated in Table 4.4, except for the 6.35 mm die roller as discussed below. Wang *et al.* (34) found that μ increased with a decrease in roller diameter but, the findings of Duncan *et al.* (15), and Bhonsle (52) indicate the opposite trend.

The slight decrease in measured coefficients of friction for the cold rolled substrate with decreasing die diameter at a constant sliding speed as seen in Table 4.4, is consistent with the findings of Duncan *et al.* (15), and Bhonsle (52). This trend has also been observed in commercial stamping operations of cold rolled sheet steels (53). With respect to the EG4 coated sheet steel the coefficients of friction were essentially independent of roller diameter.

5.4 Sliding Velocity Effects on the Coefficient of Friction

For the four roller diameters, the friction coefficient of the uncoated substrate increased slightly from 0.17 to 0.19 to 0.22 with each order of magnitude decrease in test speed. In contrast, the measured friction coefficient of the EG4 doubled for the 50.8 mm, 25.4 mm, and 12.7 mm roller diameters when the speed was reduced from 42.3 mm/s to 4.23 mm/s (*e.g.* μ=0.22 at 42.3 mm/s to μ=0.46 at 4.23 mm/s for the 12.7 mm roller). This trend of decreasing friction coefficient with increasing sliding speed is evident from the data presented in Table 4.4.

The results of this study are consistent with the findings of Nakamura *et al.* (35), Rault and Entringer (54), Sulonen *et al.* (12), and Keeler (55) who also found that the coefficient of friction decreased with an increase in sliding speed. The results obtained by Nakamura *et al.* (35) are shown in Figure 5.3. Note however that measured friction coefficients are significantly higher in this study. The materials studied include several zinc alloy coatings, a electrogalvanized zinc coated sheet steel designated as "EG", and a cold rolled steel substrate material designated as "CR" in Figure 5.3. As is evident from the data presented in Figure 5.3 the largest change observed by Nakamura *et al.* (35) in the coefficient of friction was for the electrogalvanized coating. This is the same type of material that was tested in the present study. With a decrease in strain rate at a given temperature, the strength decreases.

One theory for the decreasing values of μ with increasing sliding speed is that the lubrication regime changes with speed. This change in lubrication regime is in agreement with the Stribeck curve. A schematic drawing of a Stribeck curve for a hypothetical lubricant is presented in Figure 5.4 (32). The Stribeck curve is divided into three distinct regions: boundary lubrication, mixed lubrication and hydrodynamic lubrication. The ordinate is μ, the

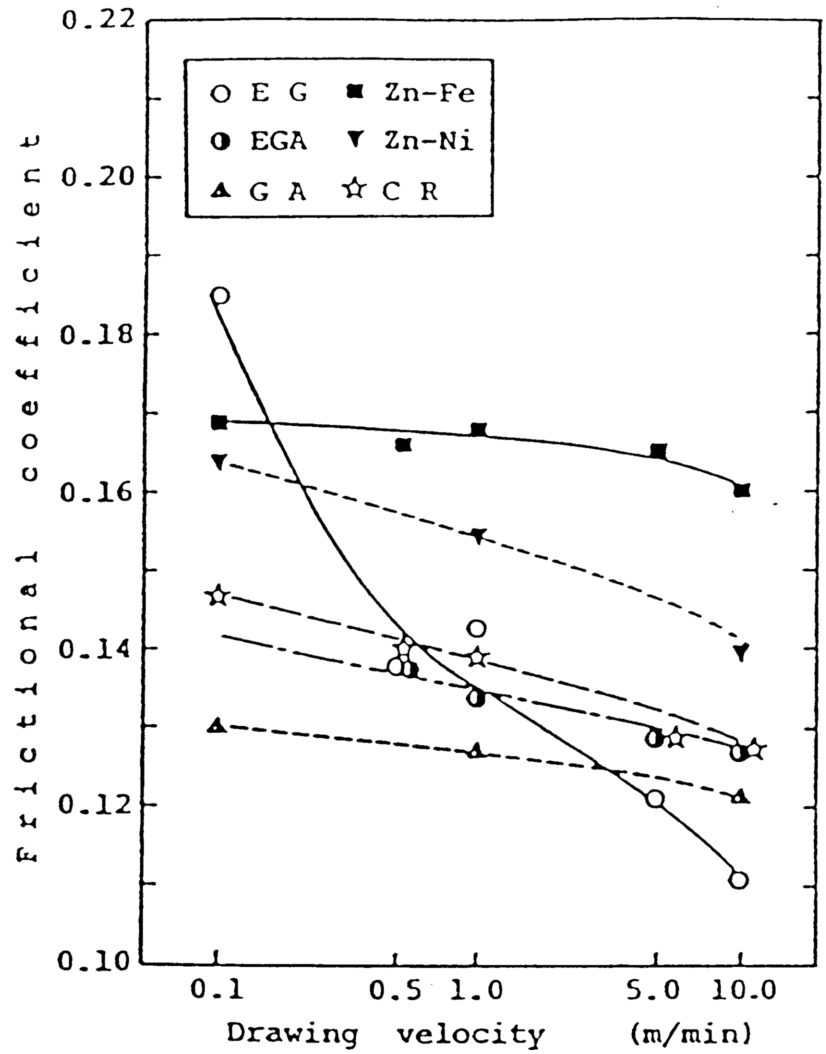

Figure 5.3 Changes in frictional coefficients with drawing velocity (35). Note the material with the most significant change in μ with speed change is an electrogalvanized material as was the case in this study.

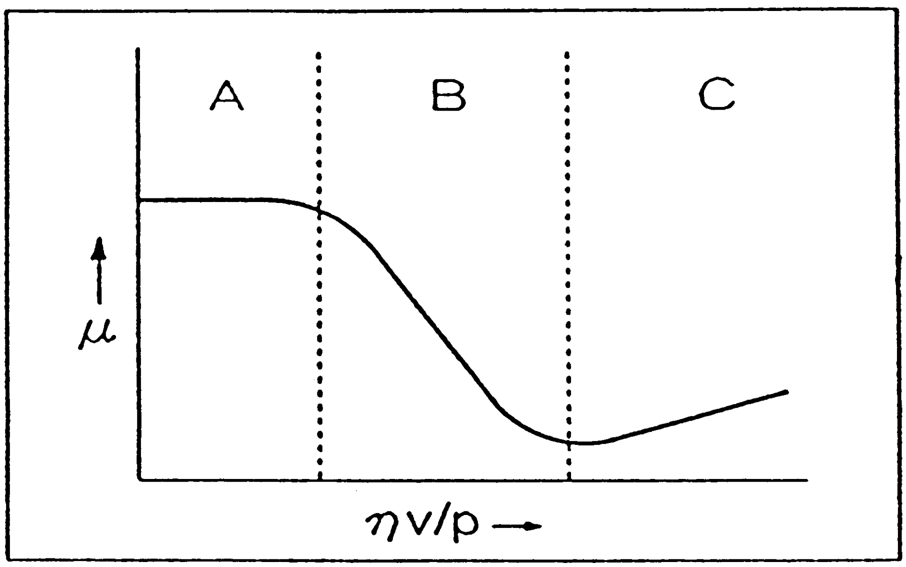

Figure 5.4 A schematic drawing of a Stribeck curve (32). The three regions: A, B and C correspond to different lubrication regimes - boundary, mixed and hydrodynamic respectively.

coefficient of friction, and the abscissa is the dimensionless parameter $\eta v/p$, where η is the viscosity of the lubricant, v is the relative interfacial velocity and p is the interfacial contact pressure. As the velocity increases, the position on the Stribeck curve is further to the right on the curve shown in Figure 5.4., thus the coefficient of friction will change with velocity.

If the Stribeck curve for the Texaco Almag lubricant used in this study is sensitive to the speed range covered (0.423 to 42.3 mm/s) then one would expect both the substrate and the EG4 to behave in a similar fashion. Since the coefficient of friction for the substrate does not exhibit the same degree of increase as the coefficient of friction for EG4, a change in lubrication regime does not explain the difference in frictional behavior between the two materials.

The fact that the frictional behavior of EG4 is extremely dependent on the test speed indicates that the presence of the electrogalvanized zinc greatly effects the measured coefficient of friction. The strain rate sensitivity of zinc may contribute to the velocity dependent frictional behavior of the EG4. The strain rate sensitivity of a zinc alloy (Zn-0.06 wt% Al-0.06 wt% Mg) is shown in Figure 5.5 as a function of homologous temperature (56). For the anticipated temperature range (*i.e.* 20°C to 100°C) of a friction test the strain rate sensitivity coefficient, m, is approximately 0.24. The effect of strain rate on the yield behavior for this zinc alloy is illustrated in Figure 5.6 as true stress verses true strain for two strain rates.

Since the coefficient of friction, as measured with the bending under tension test, is determined solely from the pulling force and the back force, the force measurements take into account the forces to overcome sliding friction as well as the force to deform the asperities on

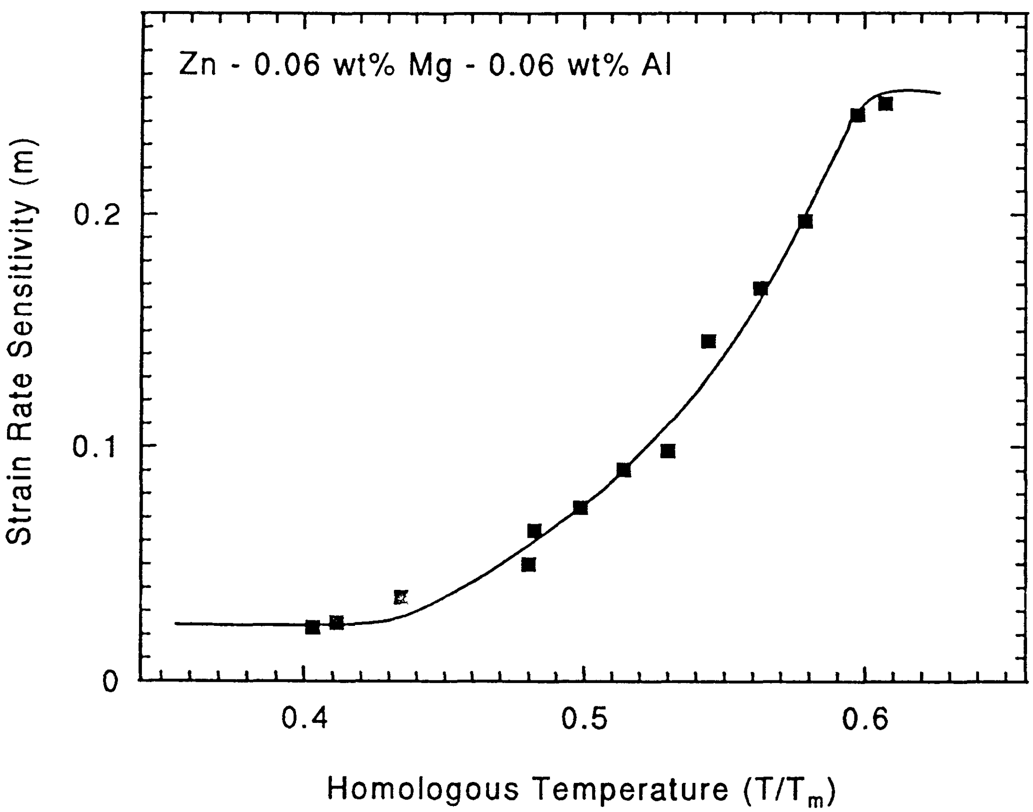

Figure 5.5 Strain rate sensitivity as a function of homologous temperature for a Zn - 0.06 wt.% Mg - 0.06 wt.% Al alloy (56).

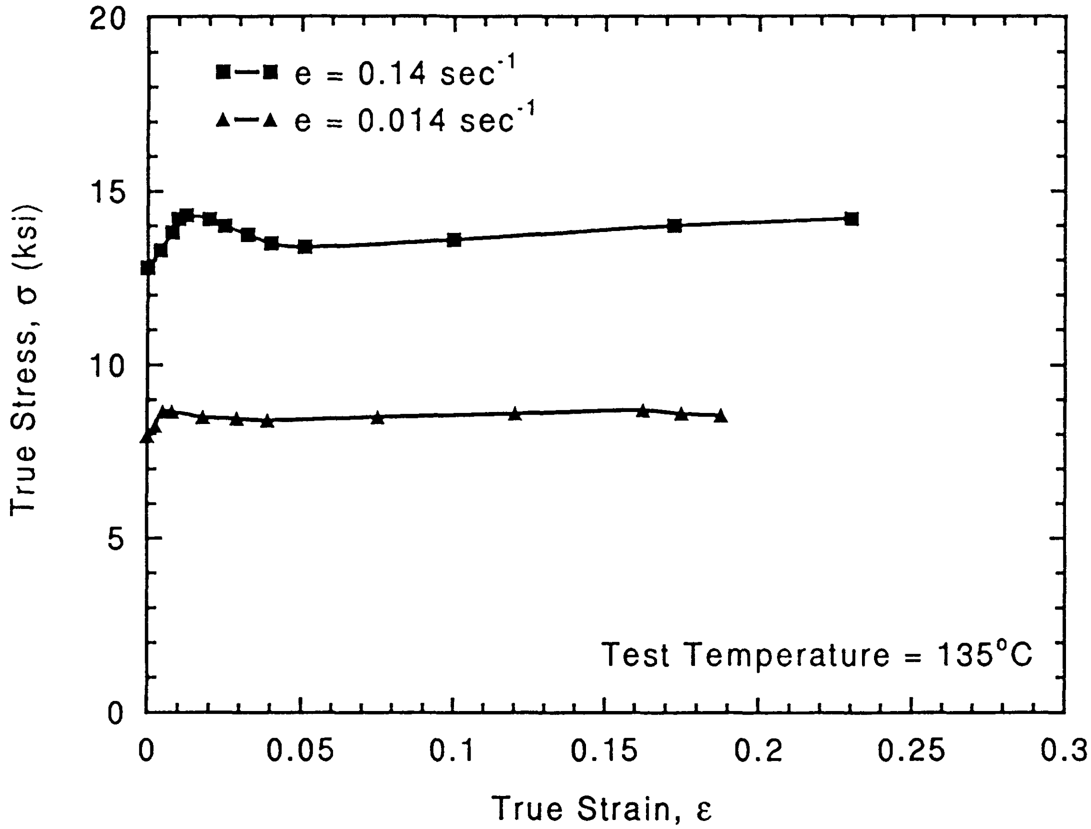

Figure 5.6 Stress - strain plots for a zinc alloy (Zn - 0.06 wt.% Mg - 0.06 wt.% Al) at two strain rates (56).

both the tool and the workpiece. Bowden and Tabor (57) indicate that the bulk material properties must be considered when examining friction and surface damage of sliding metals. The harder asperities of the steel roller plough through the softer zinc asperities, and this ploughing force is recorded as a component of the pulling force in a bending under tension test. The observations of Bowden and Tabor in combination with the strain rate sensitivity of zinc provide insight to the trend of increasing coefficient of friction with decreasing sliding speed for the EG4 as observed in this study.

As seen in Figure 5.6, the yield strength of the zinc alloy is significantly lower at a given temperature when the strain rate is decreased by an order of magnitude. This decrease in strength results in greater asperity ploughing at slower speeds. The increase in asperity ploughing results in an increased force required to move the strip relative to the die; thus, an increase in the measured coefficient of friction. The findings of Bowden and Tabor (57) also indicate that the ploughing of asperities should not be influenced by lubrication until significant displaced material has accumulated in front of the die. This accumulation of coating debris was not observed after testing on the three larger diameter rollers.

To further illustrate the effect of sliding speed on the zinc coating, the measured coefficient of friction was determined at different speeds while other test parameters (roller diameter and back force) were held constant. The effect of velocity is shown in Figure 5.7 for the EG4 material tested at three different contact pressures (*i.e.* three different roller diameters) with a constant back force of 4450 N. The trend is a decrease in the coefficient of friction with increasing sliding speed. It is also important to note that the data for the three different test pressures all fall with in the same band of friction coefficient values.

5.5 6.35 mm Diameter Roller Results

The testing with the 6.35 mm diameter roller was different from the three other diameter tests in that no free roller tests were preformed. To obtain the force required to bend the material over the 6.35 mm roller, an intercept method as proposed by Davies and Stewart (19) was used. This method assumes that the bending force F_B is a constant and independent of F_1, the pulling force. Based on these assumptions, when the back force is zero, the intercept of the best fit line through the measured data pairs is the bending force F_B. Details about this technique are described in Section 1.2. The validity of Davies and Stewart (19) method was confirmed by using this method on the other three diameter rollers and comparing the intercept value to the bending force values obtained from free roller tests.

When comparing the speed differences within the 6.35 mm roller tests several trends were noticed. As summarized in Table 4.4, the average frictional coefficient, μ, of the EG4 substrate material is essentially constant regardless of sliding speed. The frictional coefficient of the EG4 material was higher than the corresponding μ value of the substrate at a given speed. Flaking of the coating was observed at the 0.423 mm/s sliding speed on the 6.35 mm roller. This loss of zinc was seen at both low and high back forces. A photograph of the flaking EG4 coating is shown in Figure 4.5. Zinc was also found to adhere to the 6.35 mm diameter roller after each test. This coating failure is attributed to a break down of the lubricant at the interface. The effect of the low sliding speed which reduces the shear strength of the zinc combined with the high interfacial pressure causes an "avalanche" effect in the ploughing phenomenon. This "avalanche" causes the resulting coating break down which is observed in Figure 4.5. For high pressure situations similar to the one observed in

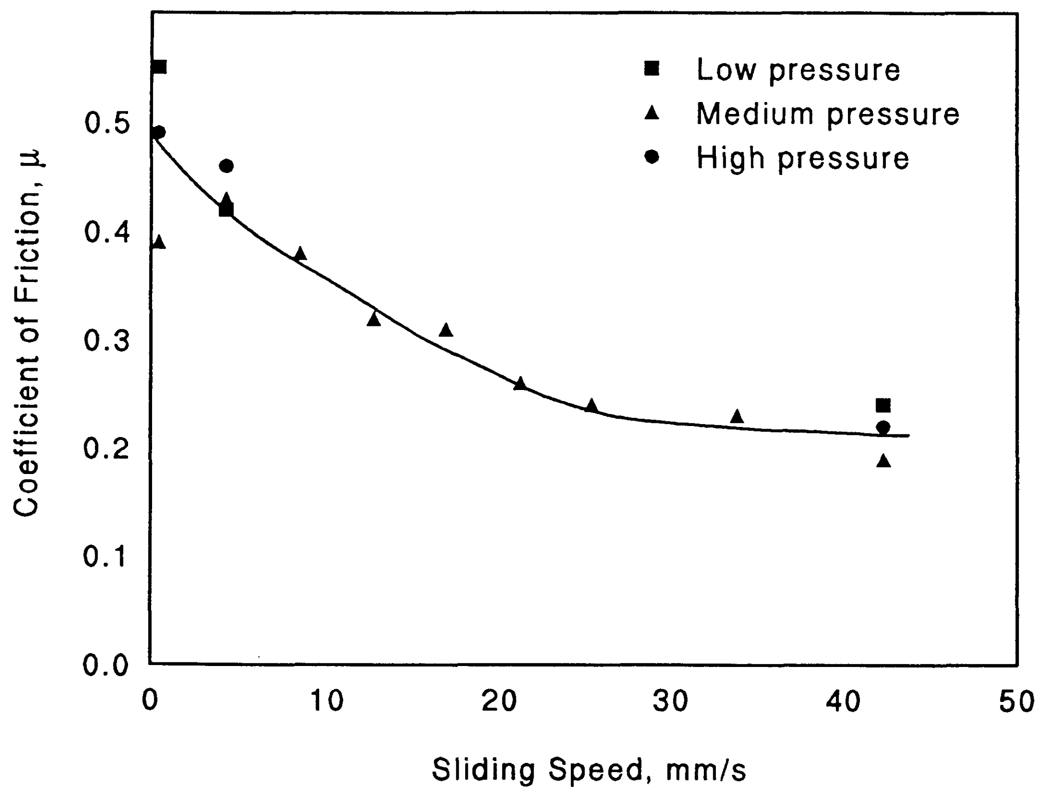

Figure 5.7 The coefficient of friction as a function of sliding speed for EG4. The applied back force was held constant while the contact pressure was controlled by the roller radius.

the 6.35 mm diameter roller tests, the constant friction factor theory may be a better model for the frictional behavior.

5.6 Pressure Considerations

The pressure at the interface between the tool and the workpiece is described by a mathematical relationship consisting of the applied forces and the geometry of the tool and work piece. The contact pressure for the bending under tension friction test is given by (2):

$$p = \frac{F_1 + F_2}{2rw} \qquad [5.5]$$

where: F_1 = measured pulling force

F_2 = measured back force

w = sheet width

2r = roller diameter

From Equation 5.5 it is obvious that the contact pressure varies inversely with roller diameter. The four rollers (6.35 mm to 50.8 mm diameter) used in this study resulted in a large range in contact pressures. The pressure ranges determined using the entire set of fixed roller data obtained for each roller at a sliding speed of 42.3 mm/s are summarized in Table 5.5. The four rollers in this study cover a pressure range of 2.1 MPa to 57.8 MPa. There is an overlap in the pressure range between each consecutive diameter roller. The maximum

Table 5.5 Contact pressure ranges for the four roller diameters employed in this study.

Roller Diameter (mm)	Pressure Range (MPa)
50.8	2.1 - 7.8
25.4	4.6 - 15.6
12.7	10.8 - 28.7
6.35	19.7 - 57.8

contact pressure obtainable at a specific roller radius is limited by the strength of the sheet steel strip.

The contact pressure at the interface between the tool and the workpiece results in asperity deformation which is most easily characterized by true contact area measurements. In Figure 5.8 the true contact area is plotted as a function of contact pressure for three different pressures and several sliding speeds at each pressure. The contact area increases with increasing pressure to what appears to be a maximum of approximately 60 percent. This observation is consistent with the findings of Wahim and Bay (45). To investigate the relationship between the coefficient of friction and the interfacial pressure, the coefficient of friction was plotted as a function of contact areas for three pressure ranges at various speeds. The results of this study are presented in Figure 5.9. From Figure 5.9 it is observed that the coefficient of friction is independent of contact area (*i.e.* contact pressure) and that the increase in μ is due primarily to the decrease in interfacial sliding speed.

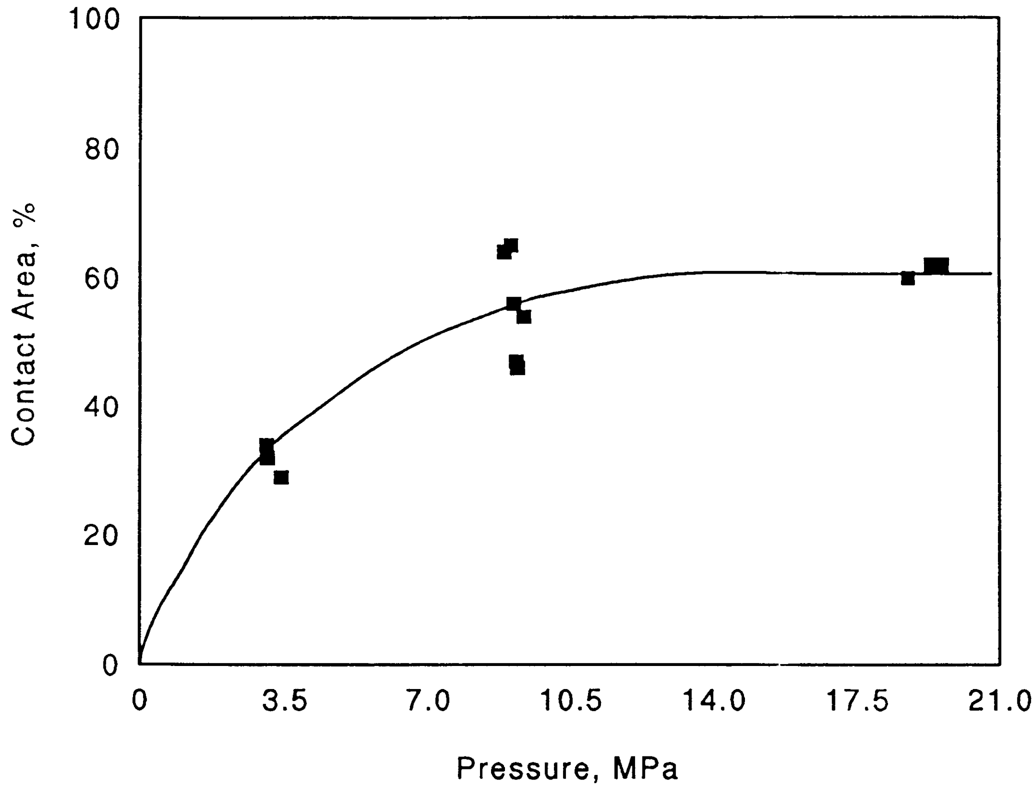

Figure 5.8 True contact area plotted as a function of contact pressure for three different pressures and various speeds.

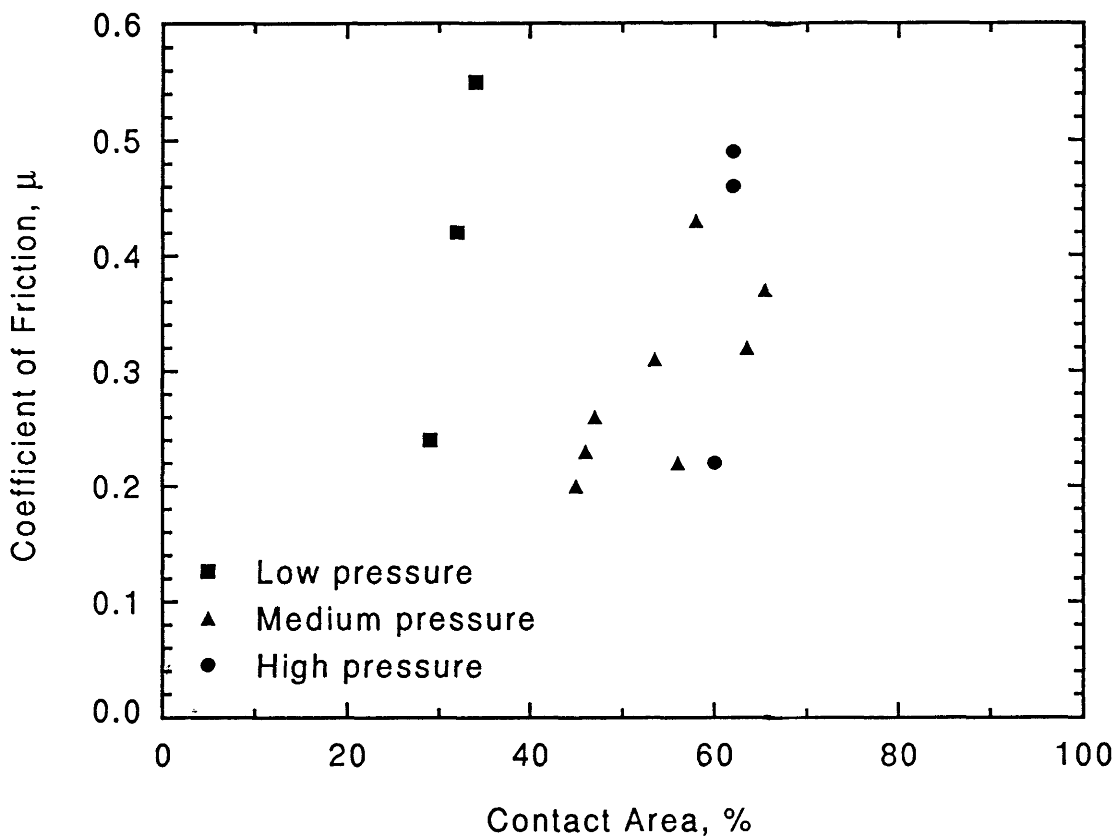

Figure 5.9 Coefficient of friction, μ, as a function of contact area for three pressure ranges.

5.7 Comparison of EG4 to Previously Studied Electrogalvanized Sheet Steels

The current results for EG4 are compared with the results from a previous study (50). The comparison is limited to a test speed of 42.3 mm/s on a roller diameter of 25.4 mm. These restrictions are due to the fact that the EG1, EG2, and EG3 materials were tested with a single roller diameter. The characteristics of the four commercially produced electrogalvanized sheet steels are presented in Table 5.1. The parameters compared in Table 5.1 are R_a, crystallographic texture, and the coefficient of friction, μ. From Table 5.1 it is seen that the roughness of the EG2 and EG4 are similar while the EG1 and the EG3 had lower and higher roughnesses respectively. The crystallographic texture of the EG1, EG2, and EG4 consisted of low angle pyramidal orientation with some basal texture on the EG1 and some high angle pyramidal texture on the EG2. The crystallographic texture of the EG3 coating consisted of prismatic and high angle pyramidal orientations. By comparing the two parameters of roughness and texture to the measured coefficient of friction a trend is observed. The roughness of the coating does not appear to influence the frictional behavior of the coating as much as the crystallographic orientation. The coefficient of friction for EG1, EG2, and EG4 is essentially the same (0.19 to 0.20) while the coefficient of friction measured for the EG3 material under the same test conditions was substantially lower (0.14). This leads to the observation that the texture and corresponding mode of coating deformation plays a role in the frictional behavior of electrogalvanized sheet steel.

5.8 Implications to Production Operations

The speed dependance of μ for the electrogalvanized sheet steel leads to several important implications to manufacturing. During a forming operation on a mechanical press the relative velocity between the tool and sheet spans a vast range, reaching a maximum at mid stroke and approaching zero at the end of the stroke. It is anticipated that as a result of the rate dependance of μ, local constraint to flow can develop and may lead to failure in regions where deformation models which only incorporate a constant rate-independent μ may predict safe deformation conditions.

6.0 CONCLUSIONS

The analysis of the friction results leads to several summary observations:

- The uncoated substrate steel has a friction coefficient that is essentially constant for a specific test speed but increases slightly as the speed is decreased.
- The friction coefficients for the EG4 coated sheet steel are independent of roller diameter but increases significantly with a decrease in sliding speed.
- The displacement rate dependance of the coefficient of friction for the electrogalvanized material may lead to localized constraint and failure in stamping operations.

These observations are attributed to the strain rate sensitivity of the zinc coating in the temperature range of the friction test. As the test speed increases, the higher yield strength of the zinc allows less plastic deformation which result in less ploughing of the zinc metal. Since the ploughing is reduced the measured friction force is also reduced. It is this reduction in the measured friction force which results in a lower coefficient of friction, μ, with increasing sliding speed.

7.0 REFERENCES

1. Schey, J.A., *Tribology in Metalworking*, ASM, Metals Park, OH, 1983, pp. 36-40.

2. Vallance, D.W., "Analysis of Friction Behavior of Coated Sheet Steel Using the Bending Under Tension Test", M.S. Thesis No. T-3796, Colorado School of Mines, Golden, CO, 1990.

3. Wenzloff, G.J., "The Importance of Microstructure and Properties in Electrogalvanized Coatings on the Formability of Sheet Steels", M.S. Thesis No. T-4288, Colorado School of Mines, Golden, CO, 1992.

4. Rangarajan, V., "Effects of Coating Properties on The Formability of Coated Sheet Steels", *Ph.D.* Dissertation T-3809, Colorado School of Mines, Golden, CO, 1989.

5. Meuleman, D.J., Denner, S.G. and Cheng, F.L., "The Effect of Zinc Coatings on the Formability of Automotive Sheet Steels", SAE Technical Paper No. 840370, SAE, Warrendale, PA 1984.

6. *American Heritage Dictionary*, 2[nd] College Edition, Houghton Mifflin Company, Boston, MA, 1985, P. 534.

7. Van Tyne, C.J., Private Communication, Golden, CO, 1993.

8. Dieter, G., *Mechanical Metallurgy*, 3rd ed., McGraw-Hill, New York, NY, 1986, pp. 544-545.

9. Wojtowicz, W.J., "Sliding Friction Test for Metalworking Lubricants", Lubrication Engineering, Vol. 11, 1955, p. 174-177.

10. Nine, H.D., "Friction Measurement for Forming of Zinc-Based Coated Sheet Steel", in *Zinc-Based Steel Coating Systems: Metallurgy and Performance*, edited by Krauss, G. and Matlock, D.K., TMS, Warrendale, PA, 1990, pp. 233-242.

11. Marciniak, Z. and Duncan, J., *Mechanics of Sheet Metal Forming*, Edward Arnold, England, 1992.

12. Sulonen, M., Eskola, P., Kumpulainen, J. and Ranta-Eskola, A., "A Reliable Method for Measuring the Friction Coefficient in Sheet Metal Forming", IDDRG Working Group Meetings, Paper WG III/4, Tokyo, Japan, 1981.

13. Vallance, D.W. and Matlock, D.K., "Application of the Bending Under Tension Friction Test to Coated Sheet Steel", Journal of Materials Engineering and Performance, Vol. 1, 1992, pp. 685-693.

14. Ranta-Eskola, A., Kumpulainen, J. and Sulonen, M., "Comparison of Strip Drawing Tests Used for Measuring Surface Interactions in Press Forming", Proceedings of 12th Biennial Congress IDDRG, 1982, p. 165.

15. Duncan, J.L., Shabel, B.S. and Filho, J.G., "A Tensile Strip Test for Evaluating Friction in Sheet Metal Forming", SAE Technical Paper No. 780391, SAE, Warrendale, PA, 1978.

16. Haruff, J.P., Hylton, T.A., Van Tyne, C.J. and Matlock, D.K., "Frictional Response of Electrogalvanized Sheet Steels", in *The Physical Metallurgy of Zinc Coated Steels: Processing, Structure, and Properties*, edited by Marder, A.R., TMS, Warrendale, PA, 1993, pp.295-307.

17. Hylton, T.A., Van Tyne, C.J. and Matlock, D.K., "Frictional Behavior of Electrogalvanized Sheet Steels", SAE Technical Paper No. 930809, SAE, Warrendale, PA, 1993.

18. Wenzloff, G.J., Hylton T.A. and D.K. Matlock, "A New Test Procedure for the Bending Under Tension Friction Test", Journal of Materials Engineering and Performance, Vol. 1, 1992, pp. 609-613.

19. Davies, R.G. and Stewart, W.S., "Influence of Die Material upon the Coefficient of Friction of Zinc Coated Steels", in *Zinc-Based Steel Coating Systems: Metallurgy and Performance*, edited by Krauss, G. and Matlock, D.K., TMS, Warrendale, PA, 1990, pp. 243-250.

20. _____________, "The Forming of Galvanized Sheet Steels - Guidelines for Automotive Applications", AISI No. SG539 0286-10-M-RI, American Iron and Steel Institute, .

21. Rangarajan, V., Giallourakis, N., Matlock, D.K. and Krauss, G., "The Effect of Texture on Deformation of Zinc Coatings", Journal of Materials Shaping Technology, Vol. 6, 1989, pp 217-227.

22. Rangarajan, V., Matlock, D.K. and Krauss, G., "The Effect of Coating Properties on the Frictional Response of Zinc-Coated Sheet Steels", in *Zinc-Based Steel Coating Systems: Metallurgy and Performance*, edited by Krauss, G. and Matlock, D.K., TMS, Warrendale, PA, 1990, pp. 263-280.

23. Shaffer, S.J., "Micromechanisms of Friction in Electrogalvanized Sheet Steel with Emphasis on the Role of Texture", *Ph.D.* Thesis LBL-29960, University of California, Berkeley, CA, 1990.

24. Shaffer, S.J., Morris Jr., J.W. and Wenk, H.R., "Textural Characterization and Its Applications on Zinc Electrogalvanized Steels", in *Zinc-Based Steel Coating Systems: Metallurgy and Performance*, edited by Krauss, G. and Matlock D.K., TMS, Warrendale, PA, 1990, pp. 129-140.

25. Kumpulainen, J.O., "Factors Influencing Friction and Galling Behavior of Sheet Metals", Proceedings of the 12th Biennial Congress, IDDRG, 1984, pp. 426-490.

26. Wenzloff, G.J., Van Tyne, C.J. and Matlock, D.K., "The Importance of Microstructure and Properties in Electrogalvanized Coatings on the Formability of Sheet Steels", in *The Physical Metallurgy of Zinc Coated Steels: Processing, Structure, and Properties*, edited by Marder,A.R., TMS, Warrendale, PA, 1993, pp. 275-293.

27. Buckley, D.H. and Johnson, R.L., "The Influence of Crystal Structure and Some Properties of Hexagonal Metals on Friction and Adhesion", Wear, Vol. 11, 1968, pp. 405-419.

28. Iwaya, J., Okano, Y. and Miyahara, M., "A Study on the Frictional Behavior of Coated Sheet Steels", Proceedings of the 16th Biennial Congress, IDDRG, 1990, pp. 189-195.

29. Wilson, W.D.R., Malkani, H.G. and Saha, P.K., "Boundary Friction Measurements Using a New Sheet Metal Forming Simulator", Transactions NAMRI/SME, 1991, pp. 37-42.

30. Meier, B.T. and Reissner, J., "Effect of Surface Quality of the Workpiece Material on the Frictional Behavior during Sheet Forming", Proceedings of the 16th Biennial Congress, IDDRG, 1990, p. 43.

31. Wilson, W.R.D., "Friction and Lubrication in Sheet Metal Forming",in *Mechanics of Sheet Metal Forming*, edited by Koistinen, D.P. and Wang, N.M., Plenum Press, New York, NY, 1978, pp. 157-177.

32. Emmens, W.C. "The Influence of Surface Roughness on Friction", Proceedings of 15th Biennial Congress of IDDRG, 1988, pp. 63-68.

33. Zheng, R. and Overby, D., "Strip Friction Experimental Study on Galvanized Steel Sheet", Proceedings of the 15th Biennial Congress, IDDRG, 1988, pp. 85-90.

34. Wang, X.J., Duncan, J.L. and Devenpeck, M.L., "Punch Friction Tests for Sheet Metal Forming", Journal of Applied Metalworking, Vol. 3, 1983, pp. 3-11.

35. Nakamura, S., Yoshida, M. and Nishimoto, A., "Frictional Characteristics of Coated Steel Sheets", Proceedings of the 15th Biennial Congress IDDRG, 1988, pp. 77-83.

36. Wall, C., "The Laboratory evaluation of Sheet Metal Forming Lubricants", Lubrication Engeering Vol. 40, 1984, pp. 139-147.

37. Ghosh, A.K., "A Method for Determining the Coefficient of Friction in Punch Stretching of Sheet Metals", International Journal of Mechanical Science, Vol. 19, 1977, p. 457.

38. Kotchman, D.P., Kim, I. and Lee, D., "Determination of Frictional Behavior In Sheet Metals Using Orthogonal Arrays", IDDRG Working Group #3 1/91-23.

39. von Stebut, J. and Perry, D. "Strip Drawing of Boundary Lubricated Uncoated and Precoated Steel Sheets: Friction Response and Metal Transfer as a Function of Tool Surface Parameters", Proceedings of the 15th Biennial Congress, IDDRG, 1988, Addendum pages.

40. Monfort, G., D'Haeyer, R., Defourny, J. and Leroy, V., "The Major Factors Governing Friction During Stamping Operations of Steel Sheets", IDDRG Working Group #3 3/89-4.

42. Wilson III, A. "Friction Effects on the Formability of Electrogalvanized and Hot-Dipped Automotive Sheet Steel", M.S. Thesis T-3733, Colorado School of Mines, Golden, CO, 1989.

43. Giallourakis, N., "Structure and Deformation of Zinc Coated Sheet Steels", MS Thesis T-3441, Colorado School of Mines, Golden, CO, 1987.

44. Wright, R. and Schurman, T., "Die Friction Variations in Simulated Sheet Metal Forming", Proceedings of the 16th Biennial Congress, IDDRG, 1990, pp. 113-119.

45. Wanheim, T., and Bay, N., "A Model for Friction in Metal Forming Processes", Annalls of CIRP, vol. 27, 1978, pp. 189-194.

46. ASM, *Metals Handbook*, Vol. 1, 10 ed, ASM International, Materials Park, OH, 1990.

47. Van Tyne, C.J., Private Communication, Golden, CO, 1993.

48. ASTM, "E 562 - Standard Practice for Determining Volume Fraction by Systematic Manual Point Count", *1984 Annual Book of ASTM Standards*, Vol. 3.03, ASTM, Philadelphia, PA, 1984.

49. ASTM, "E 8 - Standard Methods of Tension Testing of Metallic Materials", *1983 Annual Book of ASTM Standards*, Vol. 3.01, ASTM, Philadelphia, PA, 1983.

50. Detis, S., "Mechanisms of Coating Failures During Deep Drawing of Coated Sheet Steels", MS Thesis T-3834, Colorado School of Mines, Golden, CO, 1990.

51. Figliola, R. and Beasley, D., *Theory and Design for Mechanical Measurements*, John Wiley & Sons, New York, NY, 1991, p. 150.

52. Bhonsle, S.R. and Weinmann, K.J., "The Significance of Elastic Deformation of the Workpiece Sample in the Strip-Tension Friction Test", Transactions of NAMRI/SME, 1990, pp. 46-51.

53. Gordon, W.A., Private Communication, Torrington, CT, 1993.

54. Rault, D. and Entringer, M., "Relative Sheet/Tool Velocity: Its Influence on Friction and Forming Behavior of Coated Steels", Proceedings of the 14th Biennial Congress IDDRG, 1986, pp. 456-457.

55. Keeler, S., "Evaluating the Lubricity of Press Shop Lubricants on Various Types of Galvanized Steels", in 28th Mechanical Working and Steel Processing Conference Proceedings, ISS, Warrendale, PA, 1986, pp. 193-198.

56. Matlock D.K., Private Communication, Golden, CO, 1993.

57. Bowden, F.P. and Tabor, D., *The Friction and Lubrication of Metals*, Part 1 (1950) and Part 2 (1964), Oxford Univeserity Press, Oxford, England.

8.0 APPENDIX A

Force Plots For All Test Conditions

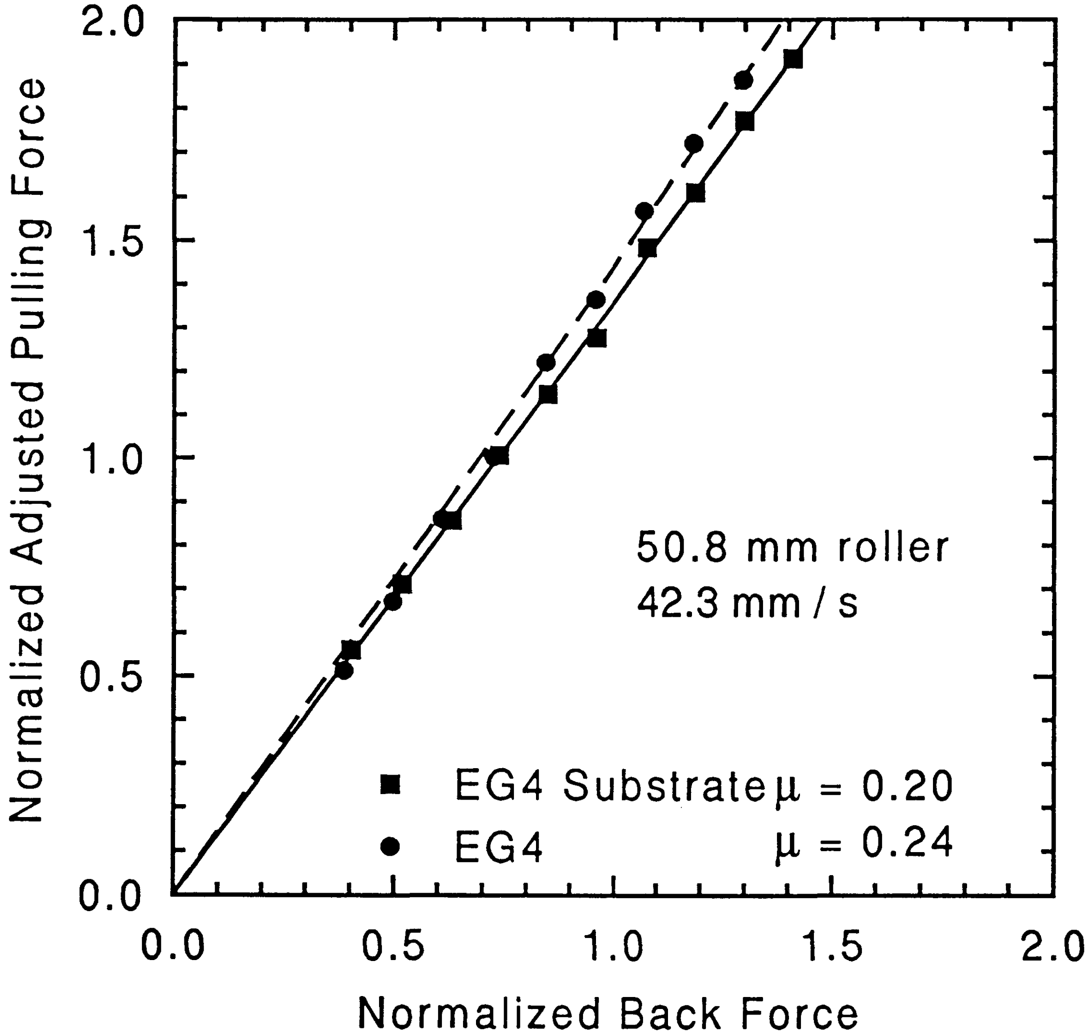

Figure 8.1 Plot of normalized adjusted pulling force versus normalized back force for both the EG4 and the steel substrate material test on the 50.8 mm roller at 42.3 mm/s.

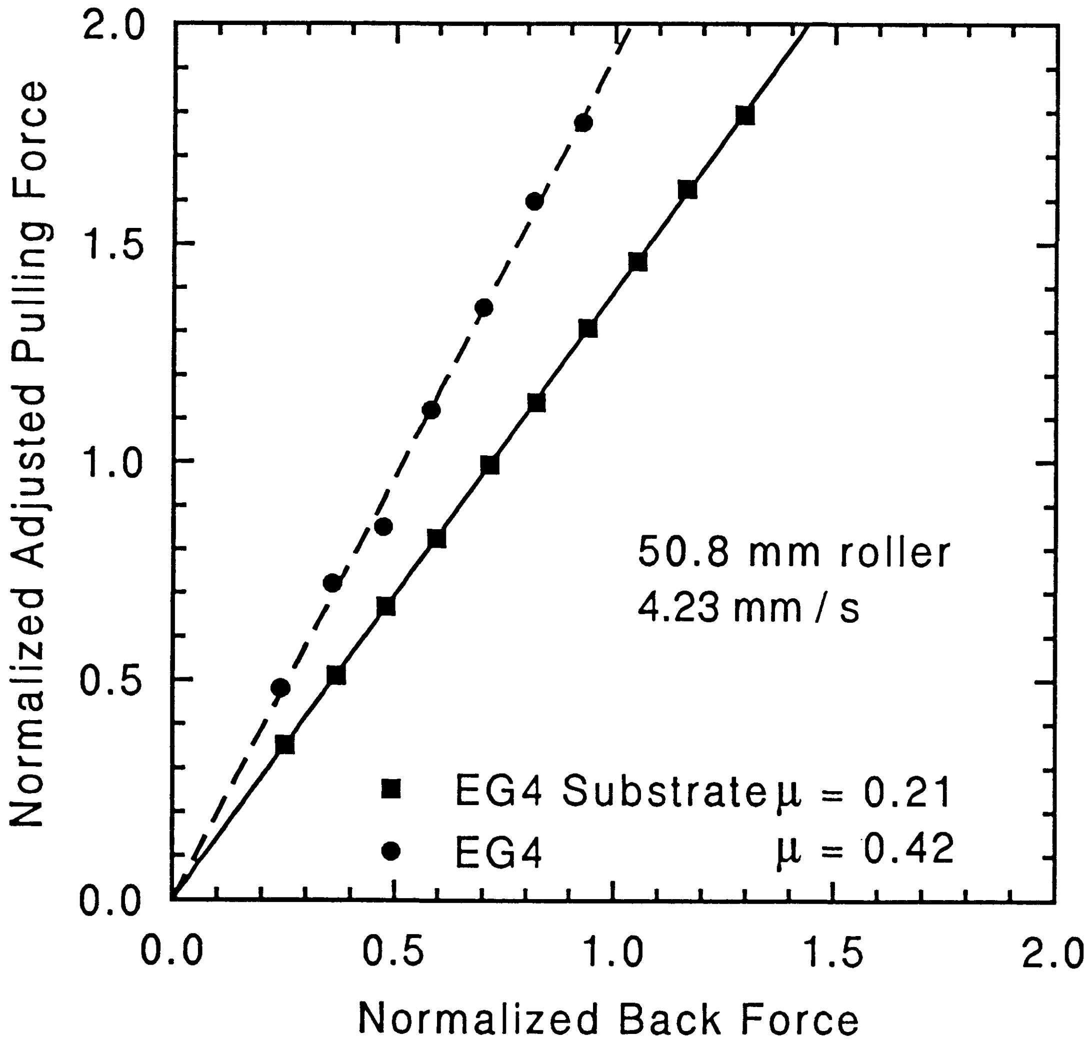

Figure 8.2 Plot of normalized adjusted pulling force versus normalized back force for both the EG4 and the steel substrate material test on the 50.8 mm roller at 4.23 mm/s.

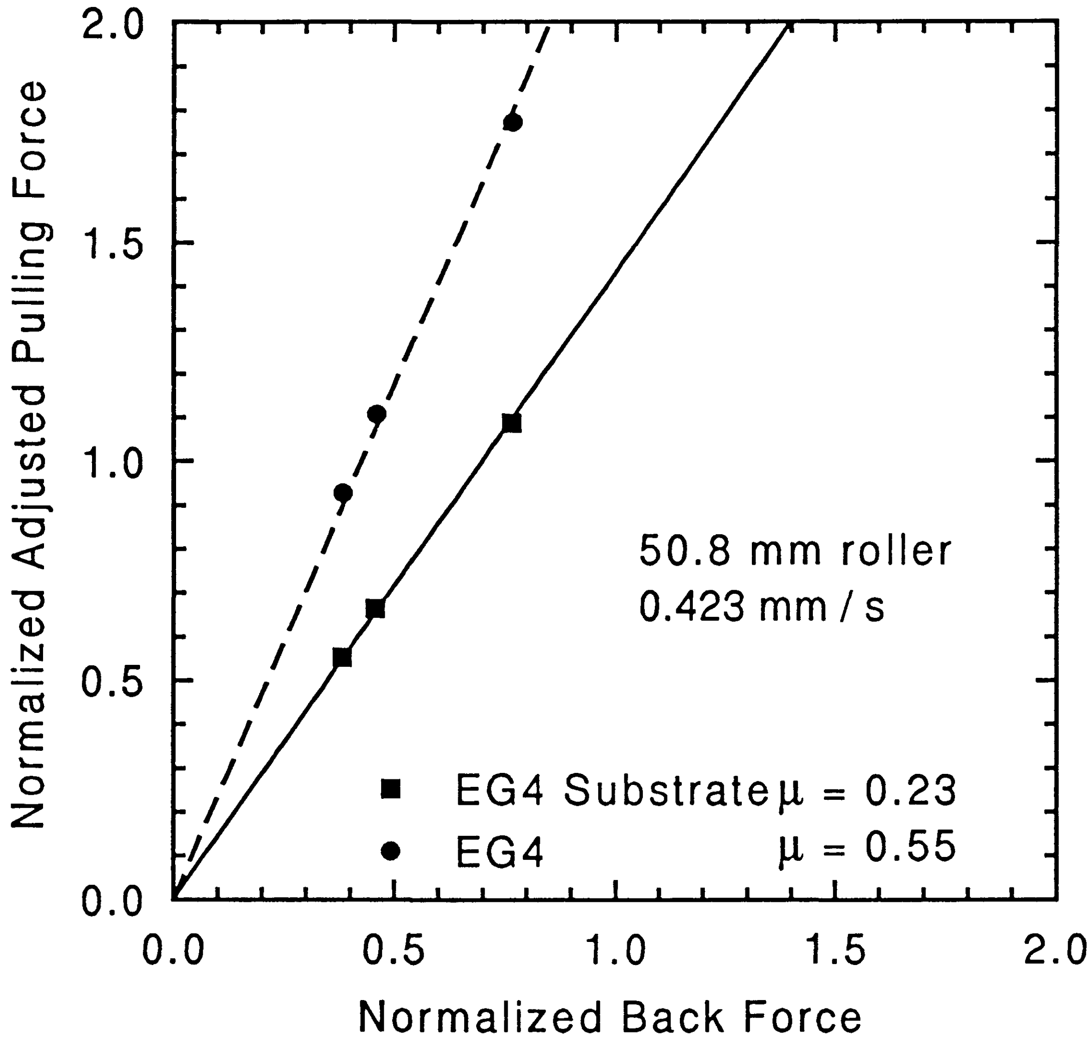

Figure 8.3 Plot of normalized adjusted pulling force versus normalized back force for both the EG4 and the steel substrate material test on the 50.8 mm roller at 0.423 mm/s.

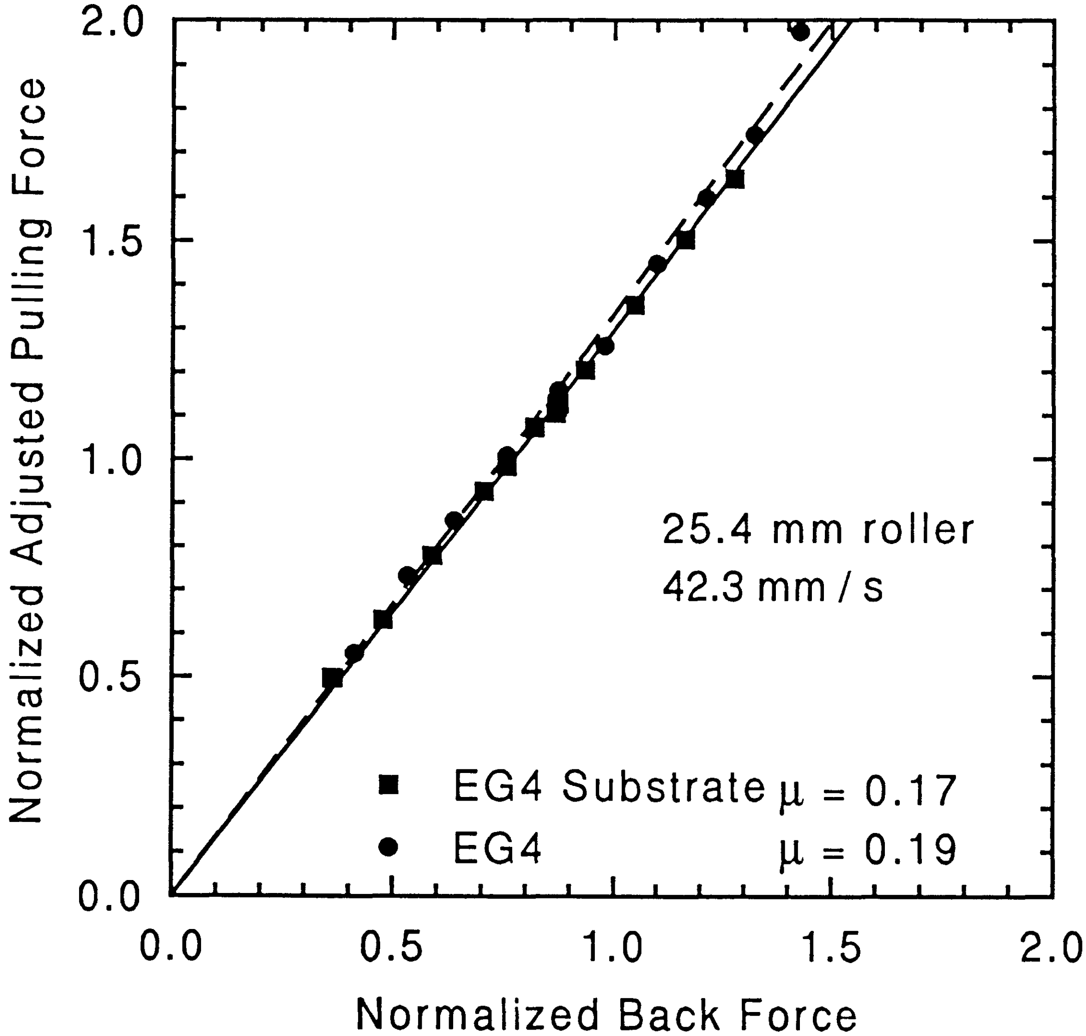

Figure 8.4 Plot of normalized adjusted pulling force versus normalized back force for both the EG4 and the steel substrate material test on the 25.4 mm roller at 42.3 mm/s.

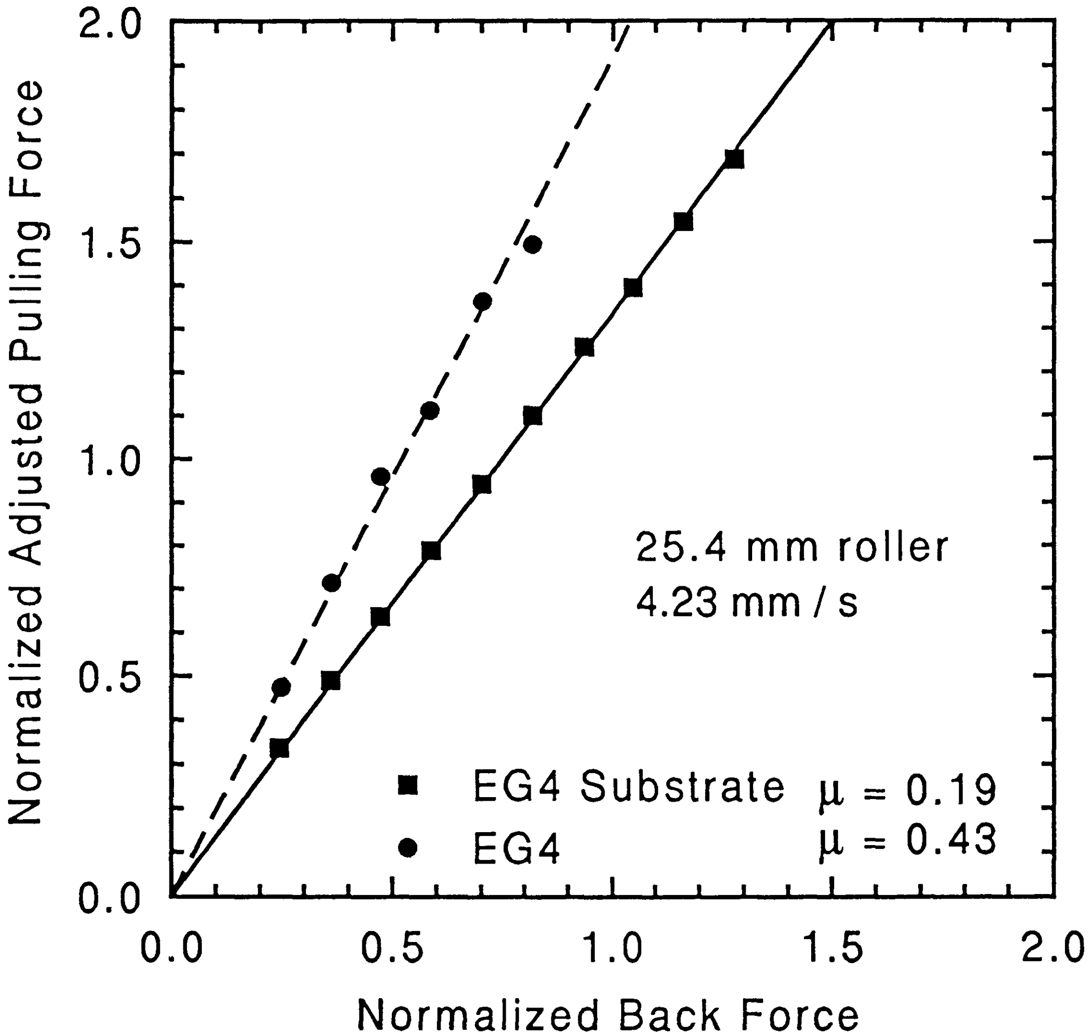

Figure 8.5 Plot of normalized adjusted pulling force versus normalized back force for both the EG4 and the steel substrate material test on the 25.4 mm roller at 4.23 mm/s.

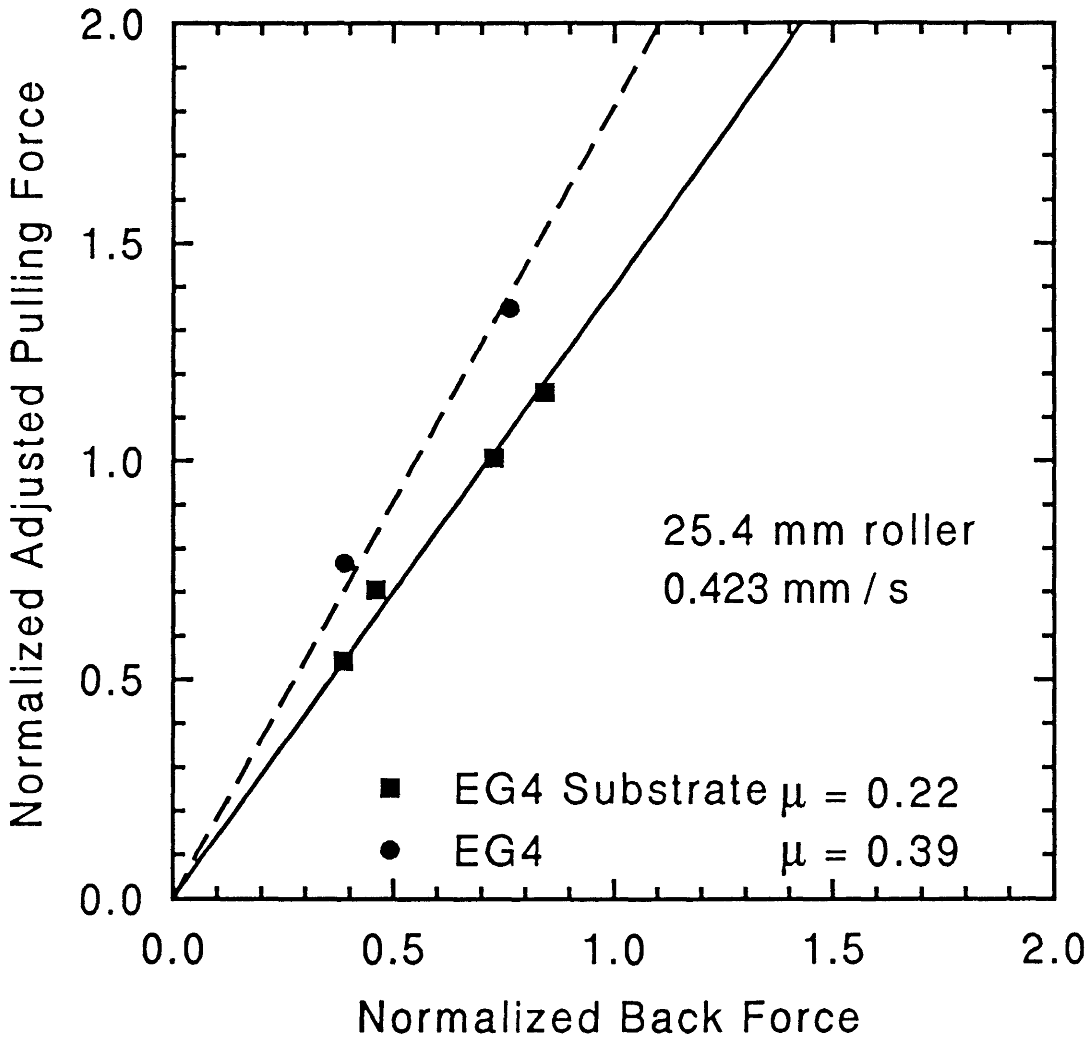

Figure 8.6 Plot of normalized adjusted pulling force versus normalized back force for both the EG4 and the steel substrate material test on the 25.4 mm roller at 0.423 mm/s.

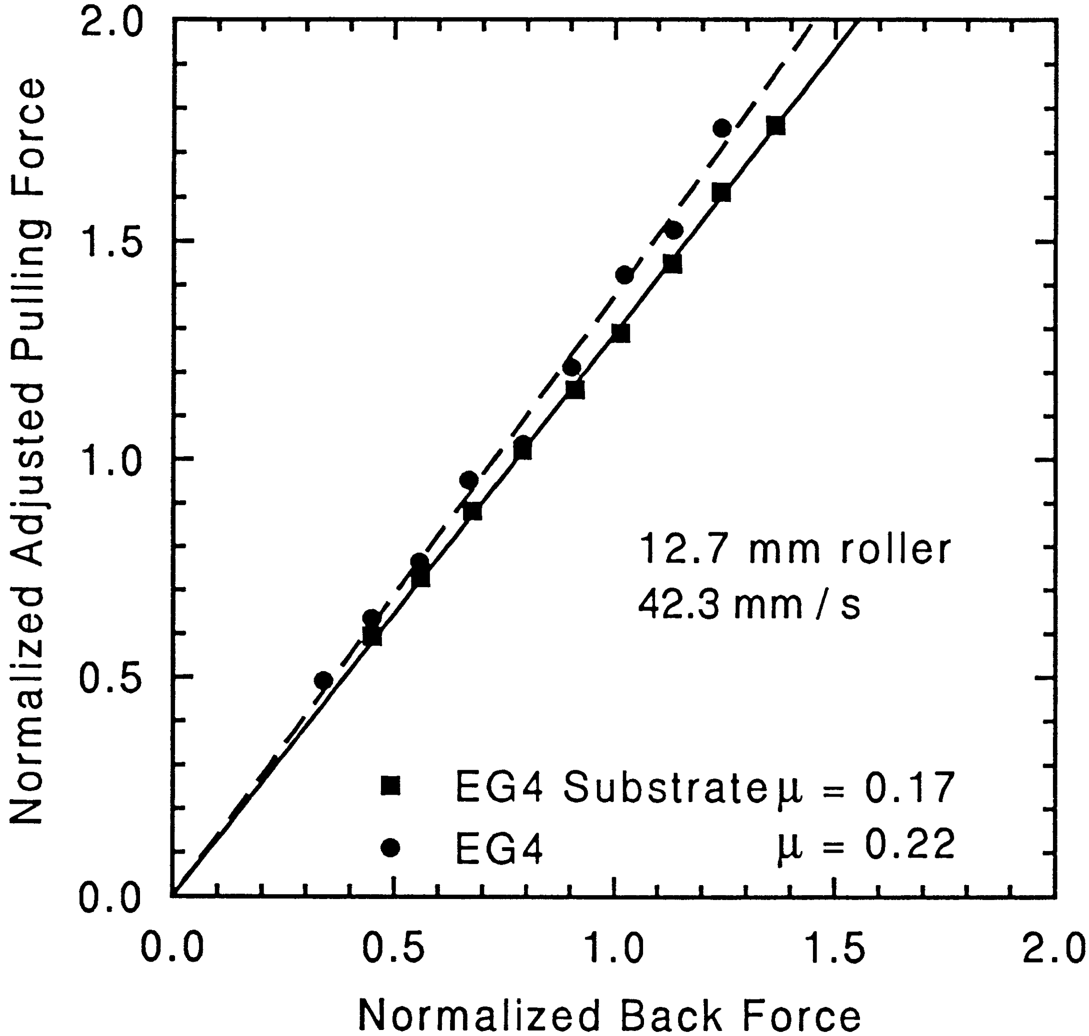

Figure 8.7 Plot of normalized adjusted pulling force versus normalized back force for both the EG4 and the steel substrate material test on the 12.5 mm roller at 42.3 mm/s.

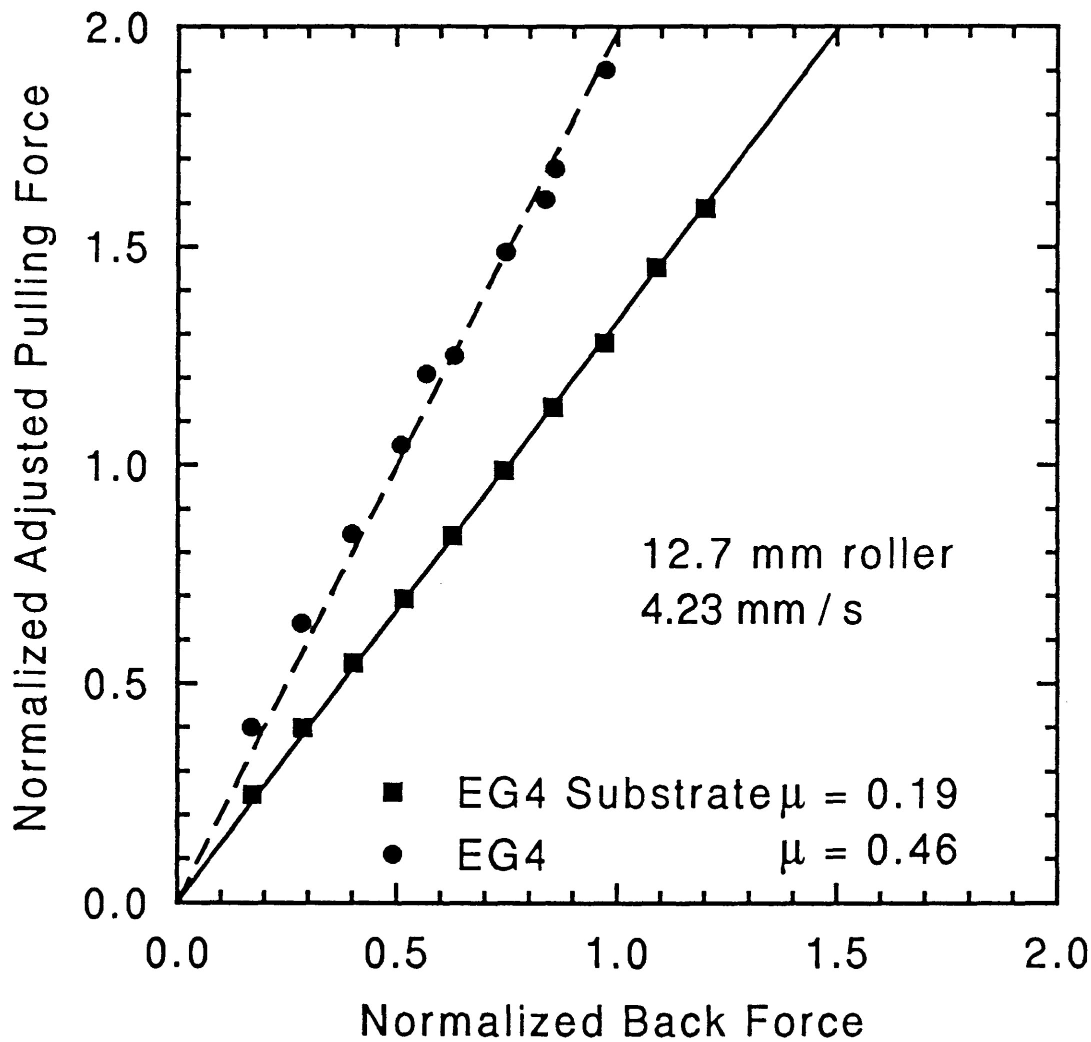

Figure 8.8 Plot of normalized adjusted pulling force versus normalized back force for both the EG4 and the steel substrate material test on the 12.7 mm roller at 4.23 mm/s.

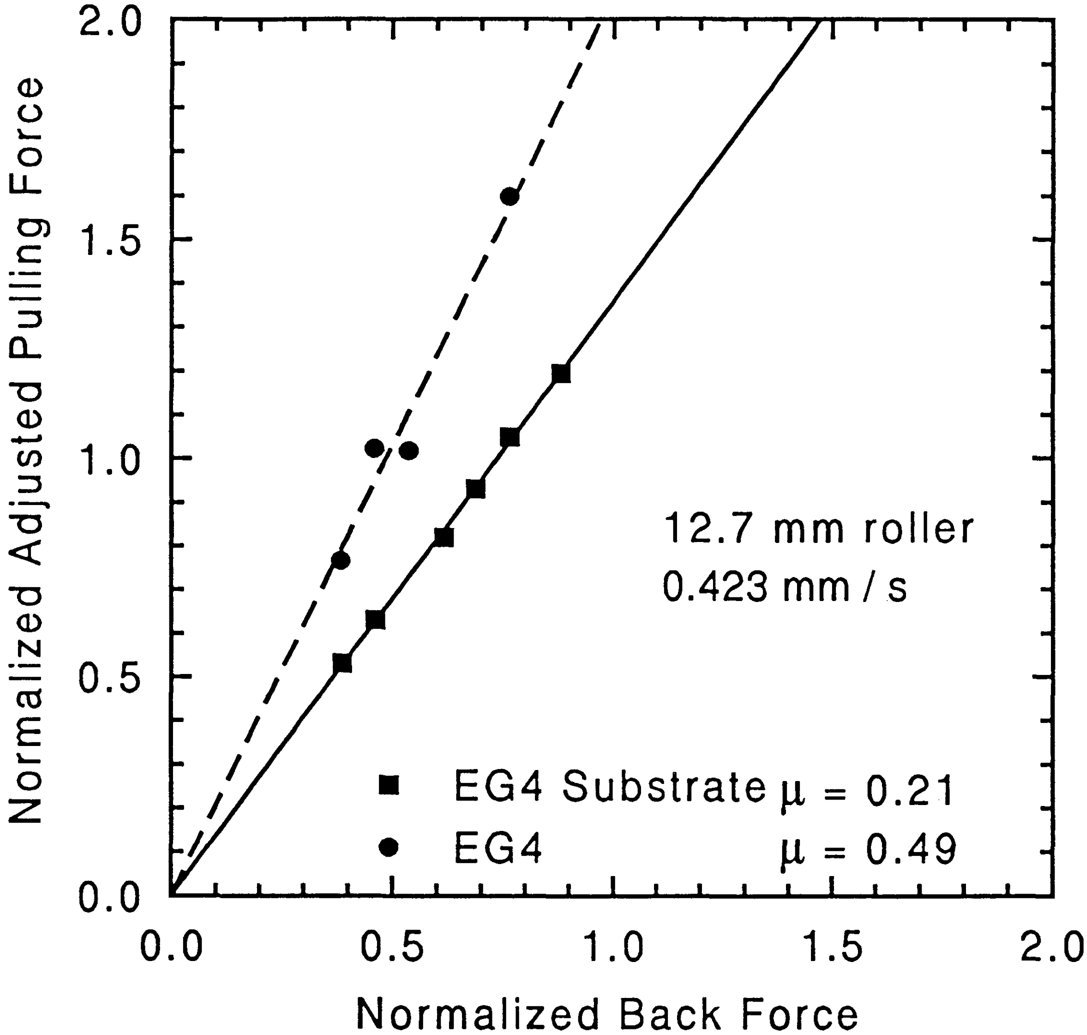

Figure 8.9 Plot of normalized adjusted pulling force versus normalized back force for both the EG4 and the steel substrate material test on the 12.7 mm roller at 0.423 mm/s.

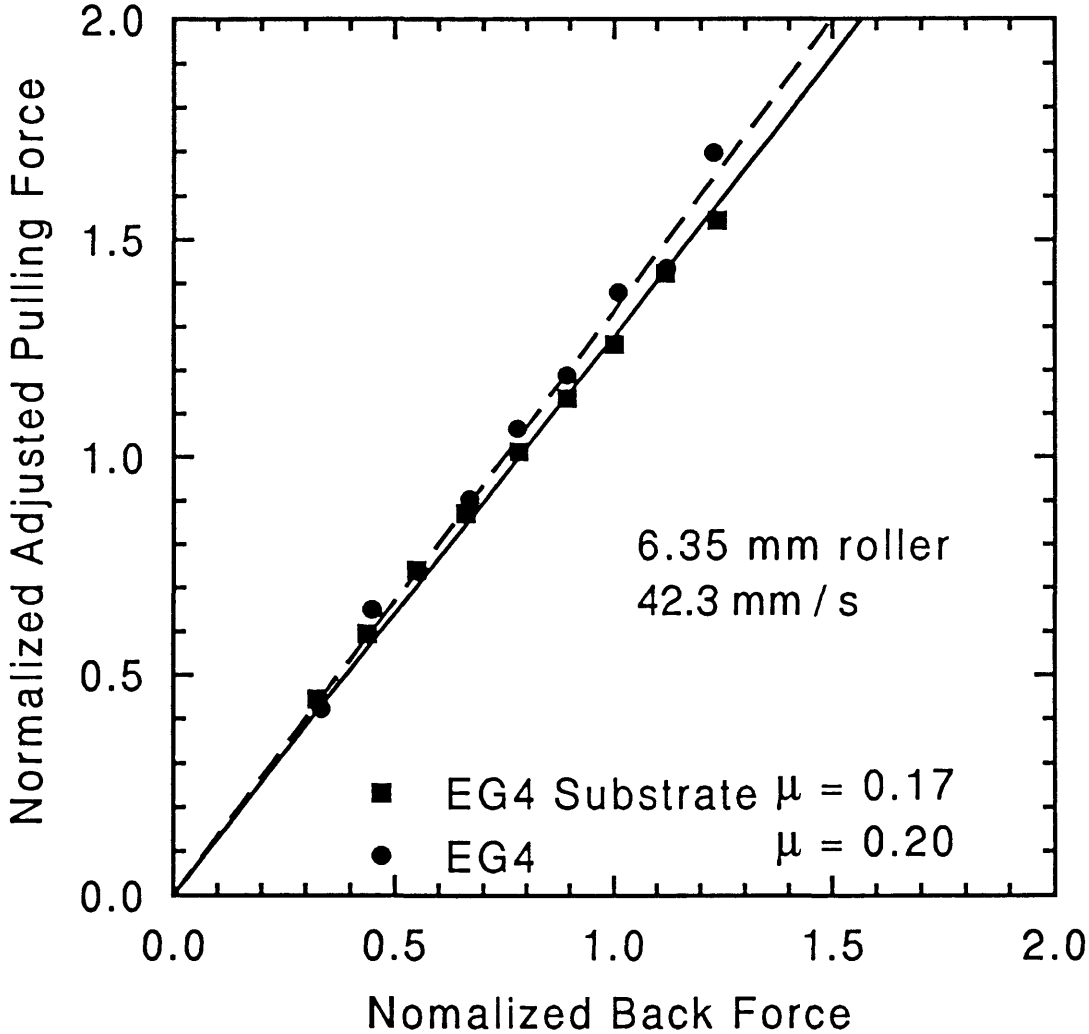

Figure 8.10 Plot of normalized adjusted pulling force versus normalized back force for both the EG4 and the steel substrate material test on the 6.35 mm roller at 42.3 mm/s.

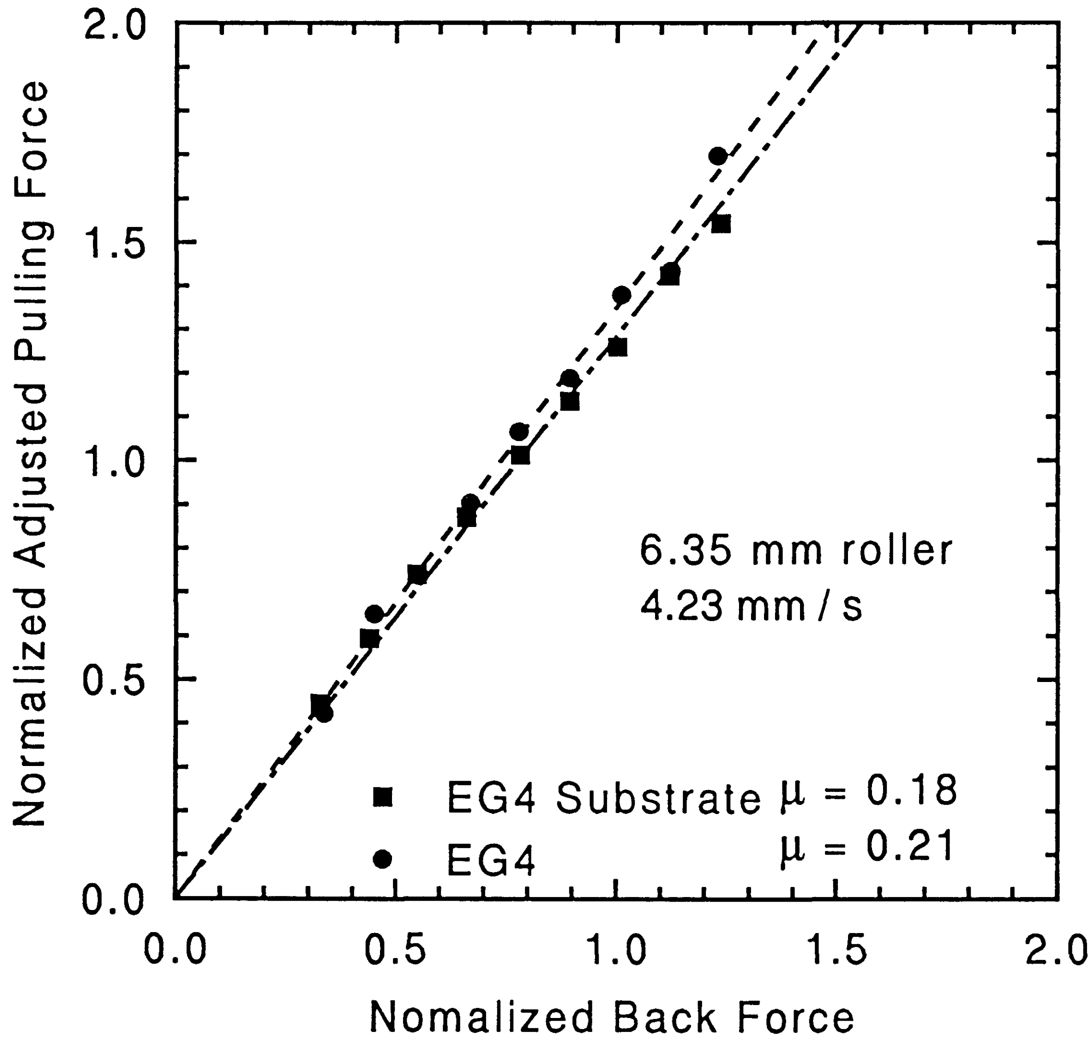

Figure 8.11 Plot of normalized adjusted pulling force versus normalized back force for both the EG4 and the steel substrate material test on the 6.35 mm roller at 4.23 mm/s.

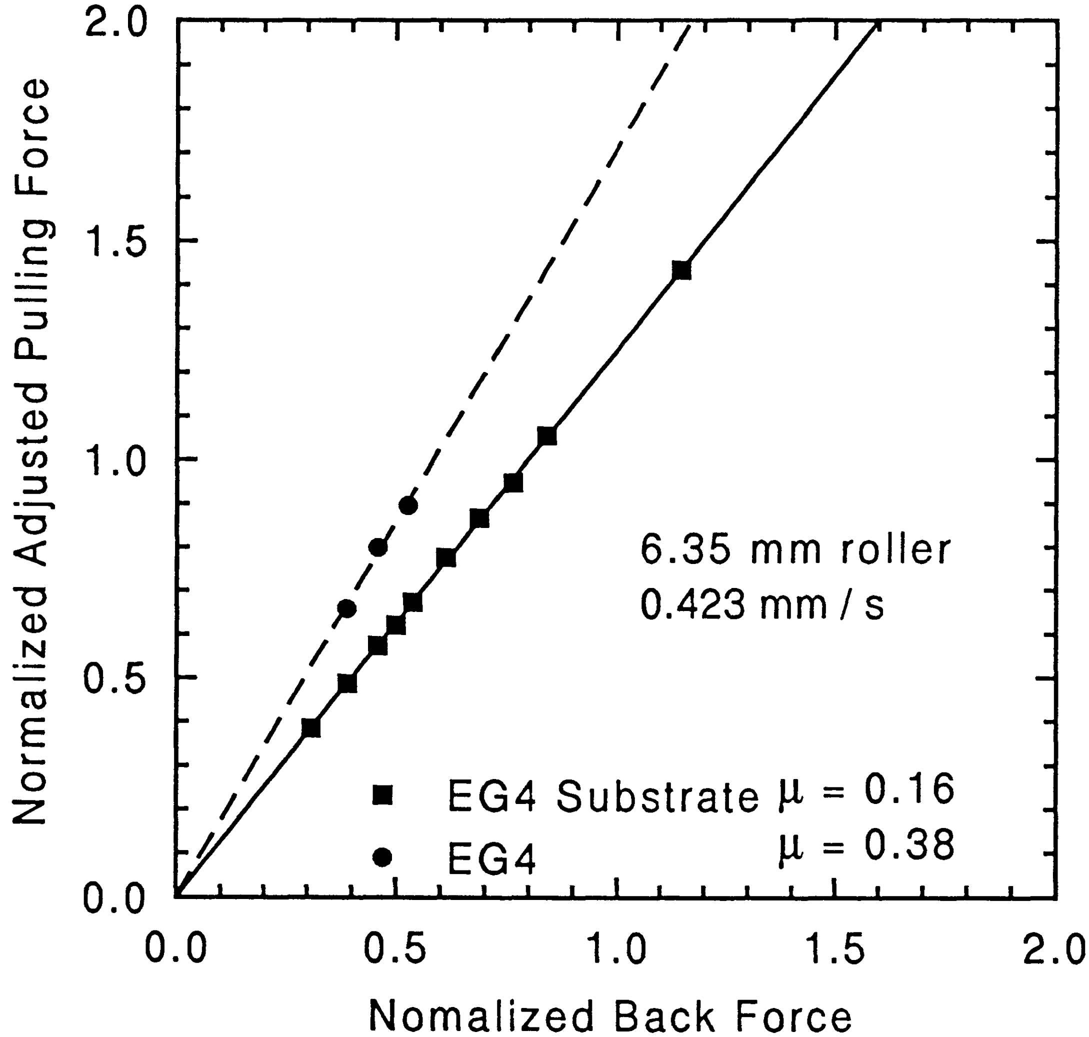

Figure 8.12 Plot of normalized adjusted pulling force versus normalized back force for both the EG4 and the steel substrate material test on the 6.35 mm roller at 0.423 mm/s.